Published OnlineFirst January 27, 2014; DOI: 10.1158/2159-8290.CD-13-0633

p-AKT depended on the presence of the EGF-like domain of CD74–NRG1 in the fusion (Fig. 3E). In addition, coculture of NIH-3T3 cells ectopically expressing CD74–NRG1 with Ba/F3 cells genetically engineered to express normal ERBB2 and ERBB3 levels also led to activation of AKT (Supplementary Fig. S7). Finally, H1568 cells ectopically expressing CD74–NRG1 exhibited enhanced colony formation in soft-agar assays (Fig. 3F; Supplementary Table S9). Taken together, these data suggest that CD74–NRG1 leads to overexpression of the EGF-like domain of NRG1 III-β3 that acts as a ligand for ERBB3, inducing its phosphorylation and subsequent activation of the downstream PI3K–AKT pathway.

DISCUSSION

We have discovered *CD74–NRG1*, a novel recurrent fusion gene in lung adenocarcinoma that arises from a somatic genomic event. Taking into account the frequencies of mutations of *EGFR* (11.3%), *KRAS* (32.2%), *BRAF* (7%), *ERBB2* (1.7%), or fusions affecting *ALK* (1.3%), *ROS* (1.7%), and *RET* (0.9%; refs. 17, 18) in lung adenocarcinomas, for which our cohort was negative, and the fact that we found 4 positive cases in our validation cohort of 102 pan-negative lung adenocarcinomas, we estimate that the frequency of *CD74–NRG1* in lung adenocarcinomas is approximately 1.7%; however, it is of note that our validation cohort was from an Asian population, so this frequency might be different in Caucasians. *CD74–NRG1* occurred specifically in invasive mucinous lung adenocarcinomas of never smokers, a tumor type that is otherwise associated with *KRAS* mutations (14). In our cohort of limited size (n = 15), *CD74–NRG1* fusions accounted for 27% of invasive mucinous lung adenocarcinomas; together, *KRAS* mutations and *CD74–NRG1* may therefore be considered the causative oncogenes in more than 60% of the cases. We provide evidence that CD74–NRG1 signals through induction of ERBB2–ERBB3 heterodimers, thus leading to PI3K–AKT pathway activation and stimulation of oncogenic growth. In light of the multitude of available drugs targeting ERBB2, ERBB3, and their downstream pathways (19), *CD74–NRG1* fusions may represent a therapeutic opportunity for invasive mucinous lung adenocarcinomas, which frequently present with multifocal and unresectable disease, and for which no effective treatment exists.

METHODS

Sample Preparation, DNA and RNA Extraction, and Illumina Sequencing

Sample preparation and DNA and RNA extraction were performed as previously described (20). RNAseq was performed on cDNA libraries prepared from PolyA+ RNA extracted from tumor cells using the Illumina TruSeq protocol for mRNA. The final libraries were sequenced with a paired-end 2 × 100 bp protocol aiming at 8.5 Gb per sample, resulting in a 30× mean coverage of the annotated transcriptome. All the sequencing was carried on an Illumina HiSeq 2000 sequencing instrument (Illumina).

Analysis of Chromosomal Gene Copy Number (SNP 6.0) and RNAseq Data

Hybridization of the Affymetrix SNP 6.0 arrays was carried out according to the manufacturers' instructions and analyzed using a previously described method (20). For the analysis of RNAseq data, we have developed a pipeline that affords accurate and efficient mapping and downstream analysis of transcribed genes in cancer samples (Fernandez-Cuesta and colleagues; published elsewhere). A brief description of the method was previously provided (20).

Analysis of Targeted Enrichment Genome Sequencing

Genomic DNA was isolated from fresh-frozen tumor tissue and subjected to CAGE Scanner analysis. This approach involves liquid-phase hybrid capture of genomic partitions enriched for genome alterations affecting 333 known cancer-associated genes (also including *CD74*). Subsequent to generation of genomic libraries from tumor DNA and capture, sequencing was performed on the Illumina platform according to the manufacturer's instructions. Significant genomic alterations were identified using approaches described previously (20).

Dideoxy Sequencing

In case of validation, sequencing primer pairs were designed to enclose the putative mutation, or to encompass the candidate rearrangement or chimeric transcript as previously described (20). Sequencing was carried out, and electropherograms were analyzed by visual inspection using four peaks.

Interphase FISH on Formalin-fixed, Paraffin-embedded Sections

Two sets of probes were prepared. One was for break-apart FISH of which probes were mapped at centromeric and telomeric regions between the break point. The other was for fusion FISH that spanned the *NRG1* and *CD74* loci. To intensify the signals, each probe was made of two or three BAC clones as follows, and the probes were labeled with SpectrumGreen and SpectrumOrange (Abbott Molecular-Vysis). Centromeric probes for break-apart FISH were RP11-1002K11 and PR11-25D16. Telomeric probes for break-apart FISH were RP11-23A12 and PR11-715M18. *NRG1* probes for fusion FISH were RP11-715H18, RP11-5713, and PR11-1002K11. *CD74* probes for fusion FISH were PR11-759G10 and PR11-468K14.

Immunohistochemistry

Immunohistochemistry was performed as previously described (21). In brief, the tissue samples were stained with p-ERBB2 (Tyr1221/1222; Cell Signaling Technology) and total ERBB1 (EGFR; Dako) at a dilution of 1:1,000 and 1:50, respectively. The Zeiss MIRAK DESK scanner was used to digitize the stained tissue. Staining for p-EGFR (Tyr1068; Cell Signaling Technology) and p-ERBB3 (Tyr1289; Cell Signaling Technology) was processed with an automated stainer (Autostainer; Dako), using the FLEX+ detection system (Dako).

Cell Culture

H2052, H322, and H1568 cells were obtained from the American Type Culture Collection and maintained in RPMI-1640 medium (Life Technologies) supplemented with 10% fetal calf serum (FCS; Gibco) and 1% penicillin–streptomycin (Gibco). The cells were cultured in a humidified incubator with 5% CO_2 at 37°C. For Western blot analysis experiments, cells were serum starved for 24 hours. NIH-3T3 cells were maintained similarly but in Dulbecco's Modified Eagle Medium (DMEM; Life Technologies). The cells were confirmed to be wild-type for *KRAS*, *EGFR*, *ERBB2*, and *ERBB3* by PCR amplification followed by Sanger sequencing of the PCR products. The cell lines have been authenticated via genotyping (SNP 6.0; Affymetrix) and tested for *Mycoplasma* contamination on a regular basis (MycolAlert; Lonza).

FACS Analysis

NIH-3T3 mouse fibroblast cells were transduced with retrovirus containing empty vector, *CD74–NRG1*, *ERBB2*, *ERBB3*, and *ERBB2+ERBB3*. H2052 cells were transduced with retrovirus

Published OnlineFirst January 27, 2014; DOI: 10.1158/2159-8290.CD-13-0633

containing empty vector or *CD74–NRG1*. Transduced cells (200,000) were washed in fluorescence-activated cell sorting (FACS) buffer (PBS, 2% FCS) and fixed in 4% paraformaldehyde for 30 minutes at room temperature. For permeabilization, cells were washed twice in Saponin buffer (PBS, 0.5% Saponin, and 2% FCS) and intracellular staining of CD74–NRG1 was performed with anti-human-CD74-PE (1:100; BioLegend). Intracellular staining of ERBB2 and ERBB3 was performed with anti-ERBB2 and anti-ERBB3 antibodies (1:50; Cell Signaling Technology). Binding of ERBB2 or ERBB3 was detected with goat-anti-rabbit-Alexa Fluor 488 (Life Technologies). Extracellular staining was performed before permeabilization with anti-human-CD74-PE and anti-NRG1 antibody (1:20; R&D Systems). Binding of the NRG1 part was detected with donkey-anti-goat-Alexa Fluor 488 (Life Technologies). Subsequently, cells were analyzed on a BD LSR II (Beckman Coulter) and quantification was assessed with FlowJo (TreeStar).

Western Blot Analysis

Immunoblotting was performed using standard procedures. The following antibodies were obtained from Cell Signaling Technology: p-AKT Ser473 (Catalog No. #9271), p-P70/S6 (Catalog No. #9205), total ERBB2 (Catalog No. #2242), p-ERBB2 (Catalog No. #2243), total ERBB3 (Catalog No. #4754), and p-ERBB3 (Catalog no. #4791). Anti-human CD74 was obtained from Abcam (Catalog No. # ab22603), and anti-polyclonal NRG1 β 1 was obtained from R&D Systems (Catalog No. AF396-NA). Actin-horseradish peroxidase (HRP) antibody was obtained from Santa Cruz Biotechnology (Catalog No. #sc47778). The antibodies were diluted in 5% BSA/TBST and incubated at 4°C overnight. Proteins were detected with HRP-conjugated anti-mouse, anti-goat, or anti-rabbit antibodies (Millipore) using enhanced chemiluminescence (ECL) reagent (GE Healthcare).

Colony Formation Assay

On a layer of bottom agar (1%), NIH-3T3 cells were suspended at low density in top agar (0.5%) containing 10% FCS, and were grown for 14 days. Subsequently, pictures were taken and systematic analyses were performed with the Scanalyzer (LemnaTec). H1568 cells were cultured under standard conditions in RPMI in 10% FCS and 1% penicillin-streptomycin. p-BABE retroviral vector inserts were confirmed via Sanger sequencing. The cells were generated by at least two independent transductions with retrovirus containing empty vector, *CD74–NRG1*, or *CD74–NRG1_* ΔEGF. After selection for 7 days with puromycin (3 μg/mL), cell lysates were taken for Western blot analysis, and cells were also used for colony formation assays as follows: on a layer of bottom agar (1.2%) cells were suspended at low density in top agar (0.6%) containing 10% FCS (final concentration), and were grown for 14 days. Subsequently, pictures were taken with a Zeiss Axiovert 40 CFL microscope at ×100 magnification, and colony size was assessed with ImageJ (http://rsbweb.nih.gov/ij/).

Generation of Ba/F3_ERBB2+ERBB3 Cells

The *ERBB2* and *ERBB3* open reading frames were amplified by PCR and cloned into the MSCV-puromycin or MSCV-neomycin vectors, respectively (Clonetech). Ba/F3 cells expressing ERBB2 and ERBB3 were generated by retroviral transduction and subsequent puromycin or/and neomycin selection. We verified the expression of the correct proteins by Western blot analysis. Ba/F3 cells were cultured in RPMI-1640 medium supplemented with 10% FBS and 1 ng/mL mouse interleukin-3.

Statistical Analyses

In Fig. 3C and F, we used a two-tailed Fisher exact test.

Disclosure of Potential Conflicts of Interest

L. Fernandez-Cuesta has ownership interest in a patent with the University of Cologne. F. Leenders is a consultant/advisory board member of Blackfield AG. M. Peifer has ownership interest (including patents) in Blackfield AG and is a consultant/advisory board member of the same. F. Malchers is a consultant/advisory board member of One. G.M. Wright has received commercial research support from Covidien and is a consultant/advisory board member of Pfizer. P. Nürnberg is CEO of ATLAS Biolabs GmbH and has ownership interest (including patents) in the same. J.M. Heuckmann is a full-time employee of Blackfield AG and is a co-founder and shareholder of the same. T. Zander is a consultant/advisory board member of Roche, Boehringer Ingelheim, Amgen, and Novartis. R.K. Thomas has received commercial research grants from AstraZeneca, EOS, and Merck KgaA; has ownership interest (including patents) in Blackfield AG and a patent application related to findings in this article; and is a consultant/advisory board member of Blackfield AG, Merck KgaA, Johnson & Johnson, Daiichi-Sankyo, Eli Lilly and Company, Roche, AstraZeneca, Puma, Sanofi, Bayer, Boehringer Ingelheim, and MSD. No potential conflicts of interest were disclosed by the other authors.

Authors' Contributions

Conception and design: L. Fernandez-Cuesta, R.K. Thomas
Development of methodology: L. Fernandez-Cuesta, R. Sun, M. Peifer, J. Altmüller, I. Lahortiga, S. Ogata, M. Parade, D. Brehmer, J. Daßler, S. Ansén, R.K. Thomas
Acquisition of data (provided animals, acquired and managed patients, provided facilities, etc.): L. Fernandez-Cuesta, D. Plenker, H. Osada, R. Menon, F. Leenders, S. Ortiz-Cuaran, M. Bos, J. Daßler, F. Malchers, J. Schöttle, R.T. Ullrich, G.M. Wright, P.A. Russell, Z. Wainer, B. Solomon, H. Nagy-Mignotte, D. Moro-Sibilot, C.G. Brambilla, S. Lantuejoul, J. Altmüller, C. Becker, P. Nürnberg, J.M. Heuckmann, E. Stoelben, J.H. Clement, J. Sänger, L.A. Muscarella, V.M. Fazio, I. Lahortiga, T. Perera, M. Parade, L.C. Heukamp, R. Buettner, T. Zander, J. Wolf, S. Perner, S. Ansén, Y. Yatabe
Analysis and interpretation of data (e.g., statistical analysis, biostatistics, computational analysis): L. Fernandez-Cuesta, D. Plenker, R. Sun, R. Menon, S. Ortiz-Cuaran, F. Malchers, J. Schöttle, R.T. Ullrich, H. Nagy-Mignotte, C.G. Brambilla, J.M. Heuckmann, I. Lahortiga, T. Perera, M. Vingron, J. Wolf, S. Ansén, S.A. Haas, Y. Yatabe, R.K. Thomas
Writing, review, and/or revision of the manuscript: L. Fernandez-Cuesta, D. Plenker, H. Osada, M. Bos, R.T. Ullrich, G.M. Wright, P.A. Russell, Z. Wainer, B. Solomon, E. Brambilla, D. Moro-Sibilot, J. Altmüller, C. Becker, P. Nürnberg, E. Stoelben, D. Brehmer, M. Vingron, R. Buettner, J. Wolf, S. Perner, S. Ansén, Y. Yatabe, R.K. Thomas
Administrative, technical, or material support (i.e., reporting or organizing data, constructing databases): L. Fernandez-Cuesta, D. Plenker, F. Leenders, S. Ortiz-Cuaran, M. Peifer, J. Daßler, F. Malchers, W. Vogel, M. Koker, G.M. Wright, P. Nürnberg, J.M. Heuckmann, I. Petersen, J.H. Clement, J. Sänger, S. Ogata, L.C. Heukamp, R. Buettner, S. Perner, S. Ansén, Y. Yatabe
Study supervision: L. Fernandez-Cuesta, Y. Yatabe, R.K. Thomas
Biobanking of tumor samples: D. Moro-Sibilot
Cell culture work, molecular biological work (e.g., PCR): M. Koker, A. la Torre
Histological review: E. Brambilla, Y. Yatabe
Laboratory work: I. Dahmen
Sample contribution: L.A. Muscarella, A. la Torre

Acknowledgments

The authors are indebted to the patients who donated their tumor specimens as part of the Clinical Lung Cancer Genome

Published OnlineFirst January 27, 2014; DOI: 10.1158/2159-8290.CD-13-0633

Project initiative. Additional biospecimens for this study were obtained from the Victorian Cancer Biobank, Melbourne, Australia. The Institutional Review Board (IRB) of each participating institution approved collection and use of all patient specimens in this study. The authors thank Philipp Lorimier, Marek Franitza, Graziella Bosco, and Juan Luis Fernandez Mendez de la Vega for their technical assistance. The authors also thank the regional computing center of the University of Köln (RRZK) for providing the CPU time on the DFG-funded supercomputer "CHEOPS" as well as for the support.

Grant Support

This work was supported by the Deutsche Krebshilfe as part of the small-cell lung cancer genome-sequencing consortium (grant ID: 109679 to R.K. Thomas, M. Peifer, R. Buettner, S.A. Haas, and M. Vingron); by the EU-Framework Programme CURELUNG (HEALTH-F2-2010-258677 to E. Brambilla, J. Wolf, and R.K. Thomas); by the Deutsche Forschungsgemeinschaft through TH1386/3-1 (to R.K. Thomas); and through SFB832 (TP5 to L.C. Heukamp; and TP6 to R.T. Ullrich, J. Wolf, and R.K. Thomas); by the German Ministry of Science and Education (BMBF) as part of the NGFNplus program (grant 01GS08101 to J. Wolf and R.K. Thomas); by the Deutsche Krebshilfe as part of the *Oncology Centers of Excellence* funding program (to R. Buettner, J. Wolf, and R.K. Thomas); by a Stand Up To Cancer Innovative Research Grant, a Program of the Entertainment Industry Foundation (SU2C-AACR-IRG60109 to R.K. Thomas); by funds of the DFG Excellence Cluster ImmunoSensation (to J. Daßler); by the Italian Ministry of Health (Ricerca Corrente RC1303LO57 and GR Program 2010-2316264) and by the "5 × 1000" voluntary contributions (to L.A. Muscarella); by the Project for Development of Innovative Research on Cancer Therapeutics (P-Direct), Ministry of Education, Culture, Sports, Science and Technology of Japan (to Y. Yatabe); by a research project grant (IWT 110431 to D. Brehmer); by the Belgium government agency for Innovation by Science and Technology (IWT; to I. Lahortiga, S. Ogata, M. Parade, T. Perera, and D. Brehmer); and by Agiradom and French Health Ministry (PPHRC; to C.G. Brambilla).

Received September 13, 2013; revised January 21, 2014; accepted January 23, 2014; published OnlineFirst January 27, 2014.

REFERENCES

1. Pao W, Hutchinson KE. Chipping away at the lung cancer genome. Nat Med 2012;18:349–51.
2. Soda M, Choi YL, Enomoto M, Takada S, Yamashita Y, Ishikawa S, et al. Identification of the transforming *EML4-ALK* fusion gene in non-small-cell lung cancer. Nature 2007;448:561–6.
3. Takeuchi K, Soda M, Togashi Y, Suzuki R, Sakata S, Hatano S, et al. *RET*, *ROS1* and *ALK* fusions in lung cancer. Nat Med 2012;18:378–81.
4. Kohno T, Ichikawa H, Totoki Y, Yasuda K, Hiramoto M, Nammo T, et al. *KIF5B-RET* fusions in lung adenocarcinoma. Nat Med 2012;18:375–7.
5. Lipson D, Capelletti M, Yelensky R, Otto G, Parker A, Jarosz M, et al. Identification of new *ALK* and *RET* gene fusions from colorectal and lung cancer biopsies. Nat Med 2012;18:382–4.
6. Chao BH, Briesewitz R, Villalona-Calero MA. *RET* fusion genes in non-small-cell lung cancer. J Clin Oncol 2012;30:4439–41.
7. Ohashi K, Maruvka YE, Michor F, Pao W. Epidermal growth factor receptor tyrosine kinase inhibitor-resistant disease. J Clin Oncol 2013;31:1070–80.
8. Camidge DR, Bang Y-J, Kwak EL, Iafrate AJ, Varella-Garcia M, Fox SB, et al. Activity and safety of crizotinib in patients with *ALK*-positive non-small-cell lung cancer: updated results from a phase 1 study. Lancet Oncol 2012;2045:11–5.
9. Bergethon K, Shaw AT, Ou S-H, Katayama R, Lovly CM, McDonald NT, et al. *ROS1* rearrangements define a unique molecular class of lung cancers. J Clin Oncol 2012;30:863–70.
10. Shaw AT, Kim D-W, Nakagawa K, Seto T, Crinó L, Ahn M-J, et al. Crizotinib versus chemotherapy in advanced *ALK*-positive lung cancer. New Engl J Med 2013;368:2385–94.
11. Hynes NE, Lane HA. ERBB receptors and cancer: the complexity of targeted inhibitors. Nat Rev Cancer 2005;5:341–54.
12. Mei L, Xiong W. Neuregulin 1 in neural development, synaptic plasticity and schizophrenia. Nat Rev Neurosci 2008;9:437–52.
13. Talmage DA. Mechanisms of neuregulin action. Novartis Found Symp 2008;289:74–84.
14. Maeda Y, Tsuchiya T, Hao H, Tompkins DH, Xu Y, Mucenski ML, et al. $KRAS^{G12D}$ and NKX2-1 haploinsufficiency induce mucinous adenocarcinoma of the lung. J Clin Invest 2012;122:4388–400.
15. Falls D. Neuregulins: functions, forms, and signaling strategies. Exp Cell Res 2003;284:14–30.
16. Wallasch C, Weiss FU, Niederfellner G, Jallal B, Issing W, Ullrich A. Heregulin-dependent regulation of HER2/neu oncogenic signaling by heterodimerization with HER3. EMBO J 1995;14:4267–75.
17. Imielinski M, Berger AH, Hammerman PS, Hernandez B, Pugh TJ, Hodis E, et al. Mapping the hallmarks of lung adenocarcinoma with massively parallel sequencing. Cell 2012;150:1107–20.
18. The Clinical Lung Cancer Genome Project (CLCGP), Network Genomic Medicine (NGM). A genomics-based classification of human lung tumors. Sci Transl Med 2013;5:209ra153.
19. Yarden Y, Pines G. The ERBB network: at last, cancer therapy meets systems biology. Nat Rev Cancer 2012;12:553–63.
20. Peifer M, Fernández-Cuesta L, Sos ML, George J, Seidel D, Kasper LH, et al. Integrative genome analyses identify key somatic driver mutations of small-cell lung cancer. Nat Genet 2012;44:1104–10.
21. Wilbertz T, Wagner P, Petersen K, Stiedl A-C, Scheble VJ, Maier S, et al. *SOX2* gene amplification and protein overexpression are associated with better outcome in squamous cell lung cancer. Mod Pathol 2011;24:944–53.

Journal of Pathology
J Pathol 2014; **233:** 402–414
Published online 16 June 2014 in Wiley Online Library
(wileyonlinelibrary.com) DOI: 10.1002/path.4377

ORIGINAL PAPER

Connective tissue growth factor and β-catenin constitute an autocrine loop for activation in rat sarcomatoid mesothelioma

Li Jiang,[1] Yoriko Yamashita,[1#] Shan-Hwu Chew,[1#] Shinya Akatsuka,[1] Shun Ukai,[1] Shenqi Wang,[1] Hirotaka Nagai,[1] Yasumasa Okazaki,[1] Takashi Takahashi[2] and Shinya Toyokuni[1*]

[1] *Department of Pathology and Biological Responses, Nagoya University Graduate School of Medicine, Japan*
[2] *Department of Tumour Biology, Nagoya University Graduate School of Medicine, Japan*

**Correspondence to: Shinya Toyokuni, Department of Pathology and Biological Responses, Nagoya University Graduate School of Medicine, 65 Tsurumai-cho, Showa-ku, Nagoya, Japan. e-mail: toyokuni@med.nagoya-u.ac.jp*

[#]These authors contributed equally to this study.

Abstract

Due to the formerly widespread use of asbestos, malignant mesothelioma (MM) is increasingly frequent worldwide. MM is classified into epithelioid (EM), sarcomatoid (SM), and biphasic subtypes. SM is less common than EM but is recognized as the most aggressive type of MM, and these patients have a poor prognosis. To identify genes responsible for the aggressiveness of SM, we induced EM and SM in rats, using asbestos, and compared their transcriptomes. Based on the results, we focused on connective tissue growth factor (*Ctgf*), whose expression was significantly increased in SM compared with EM; EM itself exhibited an increased expression of *Ctgf* compared with normal mesothelium. Particularly in SM, Ctgf was a major regulator of MM proliferation and invasion through activation of the β-catenin–TCF–LEF signalling pathway, which is autocrine and formed a positive feedback loop via LRP6 as a receptor for secreted Ctgf. High *Ctgf* expression also played a role in the epithelial–mesenchymal transition in MM. Furthermore, Ctgf is a novel serum biomarker for both early diagnosis and determining the MM prognosis in rats. These data link Ctgf to SM through the LRP6–GSK3β–β-catenin–TCF–Ctgf autocrine axis and suggest Ctgf as a therapeutic target.

Keywords: mesothelioma; sarcomatoid mesothelioma; connective tissue growth factor; β-catenin; serum marker

Received 10 November 2013; Revised 17 April 2014; Accepted 13 May 2014

No conflicts of interest were declared.

Introduction

Malignant mesothelioma (MM) is one of the most aggressive tumours, and its pathogenesis is intimately associated with asbestos exposure [1–3]. It occurs as the result of transformation of mesothelial cells that form the lubricating surfaces covering somatic cavities and most of the internal organs. In view of the long latency period of 30–40 years between exposure and disease onset, the number of patients presenting with MM is expected to rise in the coming decade [4–6]. Although MM is not common, it is a difficult cancer to treat, for the following reasons: (a) early detection is difficult, with no effective serum markers, so most cases are found at an advanced stage [7]; (b) the effectiveness of surgical procedures is limited, due to the anatomical characteristics [8]; and (c) the present chemotherapeutic regimen is not sufficiently effective [9].

MM can be subdivided into three histological subtypes: epithelioid (EM); sarcomatoid (SM); and biphasic (BM) [10]. It is occasionally difficult to differentiate SM from various other sarcomas [11,12]. Although SM is less common than EM, it is the most aggressive MM subtype, with SM patients having a remarkably short survival period [7].

We previously established a rat model of peritoneal MM with commercially used asbestos and noticed a higher incidence of SM compared to human cases [13]. Thus, this model is favourable for transcriptome analysis, with the dual aims of identifying genes responsible for the aggressiveness of SM and defining serum diagnostic and prognostic markers for MM, especially SM.

Materials and methods

Materials

We purchased the Wnt–β-catenin signalling pathway inhibitor FH353 from Sigma-Aldrich (St. Louis, MO, USA; cat. no. F5682) and the Ctgf inhibitor SA3K from Cusabio Biotech (Hubei, China). Human recombinant Ctgf was obtained from Peprotech (Rocky Hill, NJ, USA).

Carcinogenesis study using an animal model

A suspension of UICC standard asbestos in saline was prepared as described. We characterized the physical parameters of asbestos fibres [13]. F_1 hybrid rats produced by crossing female Fischer 344 and male Norway Brown rats (Charles River Japan, Yokohama, Japan) were used under specific pathogen-free conditions, and the obtained tumours and serum samples [13] were used in the present study. MM cell lines were established from the ascites present at the autopsies of rats, using the method described previously [14]. The Animal Experiment Committee of Nagoya University Graduate School of Medicine approved this study.

Gene expression microarray analysis

Total RNA was isolated using an RNeasy Mini kit (Qiagen GmbH, Hilden, Germany). A total of 28 microarrays (Whole Rat Genome Microarray, G4131F; Agilent Technologies, Santa Clara, CA, USA) were used for the screening: two microarrays were used for normal pleural mesothelial cells, two for normal peritoneal mesothelial cells and 24 for MM (13 SM, eight EM and three BM). We analysed the microarray data using GeneSpring GX 11.05.1 software (Agilent Technologies). Pathway analysis was performed for some subsets of the genes that are differentially expressed between SM and EM groups.

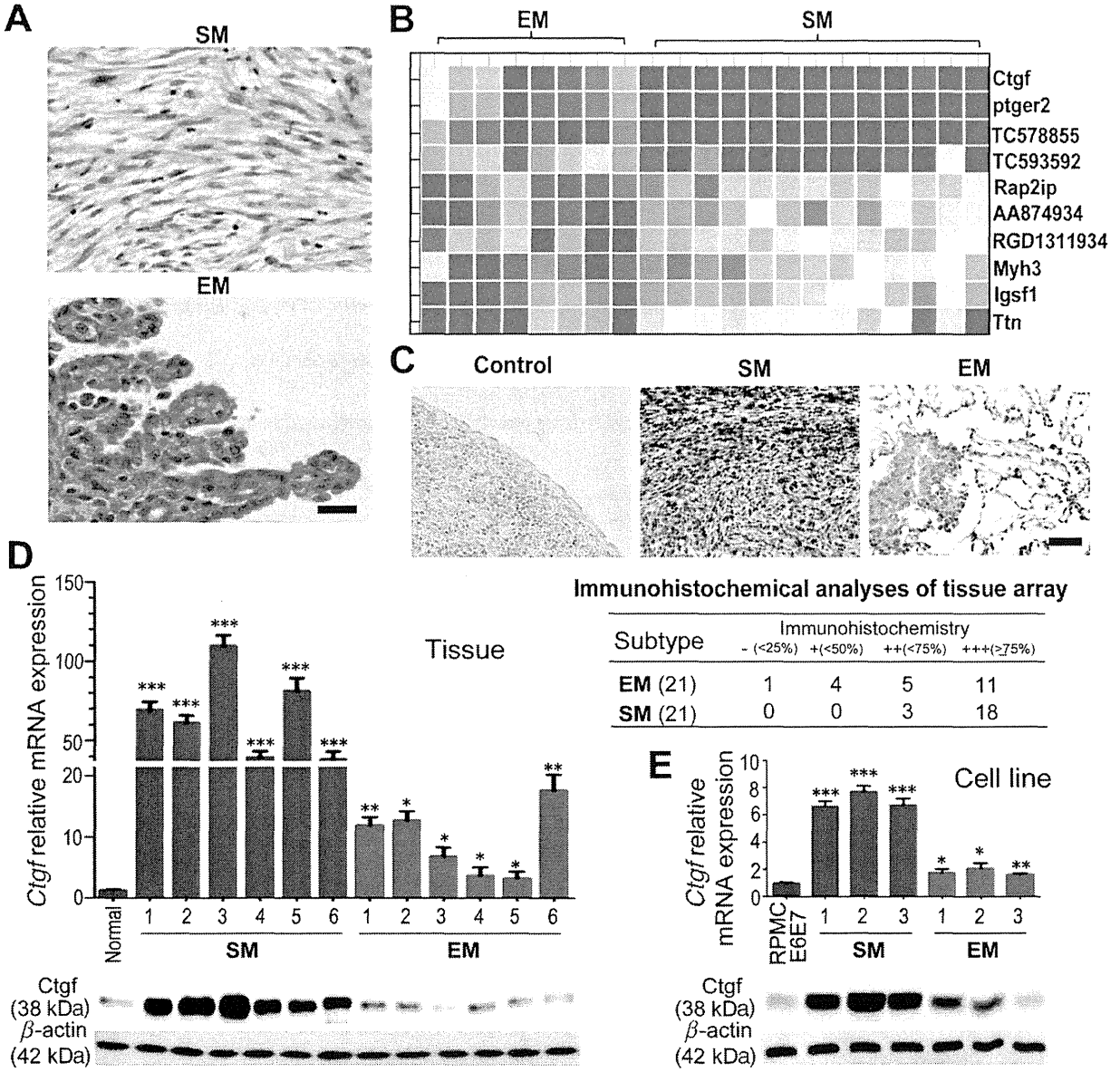

Figure 1. Differential over-expression of *Ctgf* in asbestos-induced rat MM, with a preference for the SM subtype. (A) Representative histology of SM and EM; bar = 50 μm. (B) Differential transcription between SM and EM (see also supplementary material, Figure S1, Tables S3, S4). (C) Immunohistochemical analysis of Ctgf in SM and EM with tissue arrays; bar = 100 μm. (D, E) Quantitative real-time PCR and western blot analyses of *Ctgf* in tumour tissue samples versus normal mesothelial cells (D) and in immortalized normal mesothelial cells (RPMCE6E7) versus SM and EM cell lines (E). MM, malignant mesothelioma; SM, sarcomatoid mesothelioma; EM, epithelioid mesothelioma. Results are expressed as mean ± SEM and are representative of three independent assays.

Tissue arrays, histology and immunohistochemical analysis

The tissue arrays included liver, spleen and kidney samples in each specimen. Representative areas from the tissue specimens were chosen, and cores 3 mm in diameter were punched out from the paraffin blocks using a precision instrument (Tissue Microprocessor, Azumaya, Tokyo, Japan). Twenty-four cores (6×4 array) were embedded in a paraffin block. Tissue sections with a 3 μm thickness were then stained with haematoxylin and eosin (H&E). For immunohistochemistry, the avidin–biotin complex method with peroxidase or immunofluorescence method was used as described [15–17]. Images were obtained using a BZ-9000 microscope (Keyence, Osaka, Japan).

Reverse-transcription and real-time PCR

Total RNA was isolated from the tissue samples using the RNeasy Mini kit (Qiagen). The isolated total RNA was then treated with DNase I (Invitrogen Life Technologies, Carlsbad, CA, USA) to digest residual genomic DNA. cDNA was synthesized using the First-Strand cDNA Synthesis Kit (GE Healthcare Offices, Little Chalfont, Buckinghamshire, UK) with random primers. For the real-time quantitative PCR analysis, a Platinum SYBR Green qPCR SuperMix UDG Kit

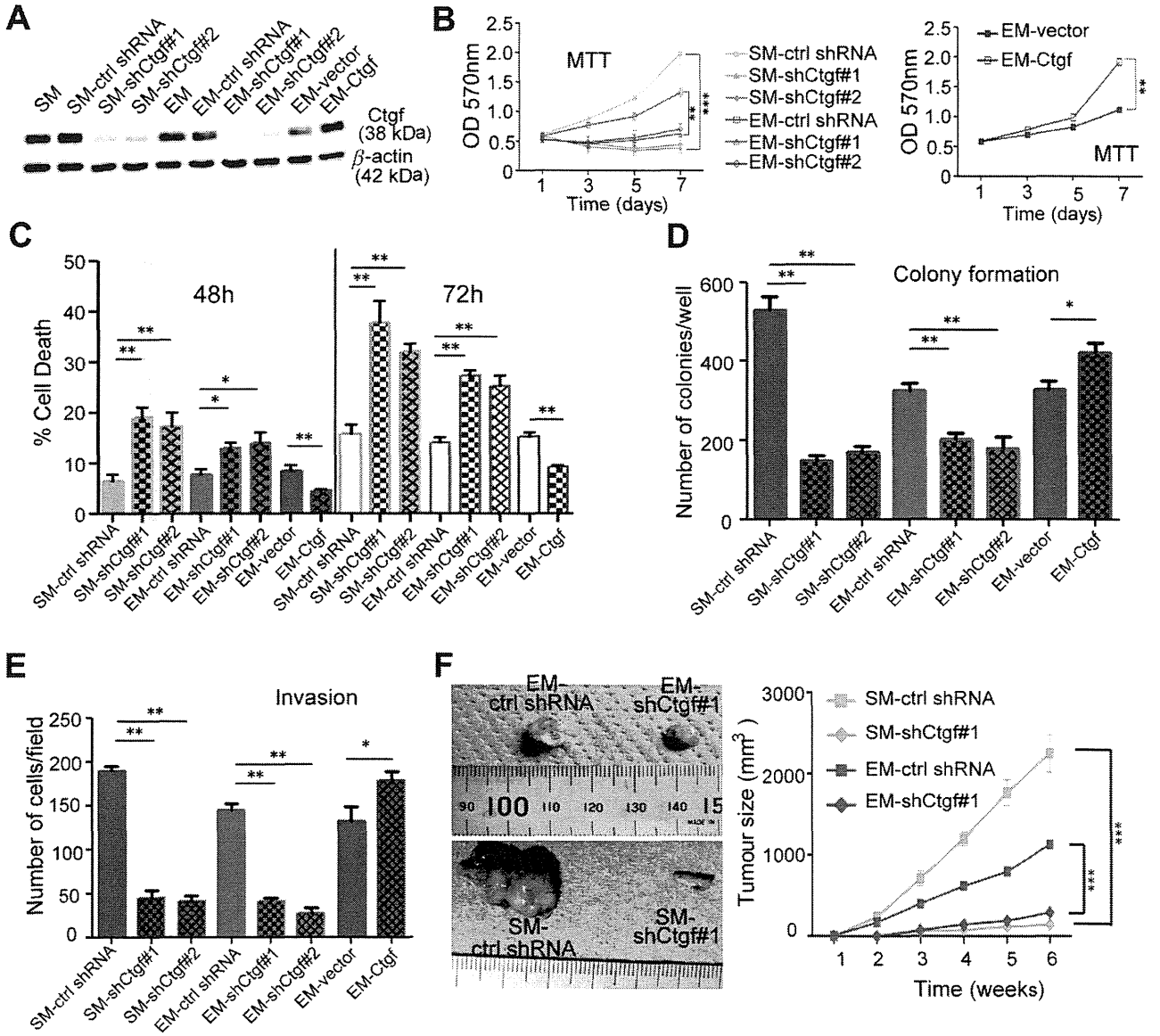

Figure 2. Malignant characteristics of rat MM cell lines depend on Ctgf. (A) Western blot analysis of Ctgf using MM cell lines after *Ctgf* transduction or knock-down. (B) MTT assay after *Ctgf* transduction or knock-down. (C) Evaluation of MM cell death with Trypan blue exclusion after *Ctgf* transduction or knock-down; cells were counted after 48 or 72 h. (D) Soft agar colony formation assay after *Ctgf* transduction or knock-down; agar was stained with 0.005% crystal violet after 14 days. (E) Invasion assays of MM cells after *Ctgf* transduction or knock-down; transwell analyses were evaluated with coated Matrigel after 24 h. (F) Tumourigenicity of control shRNA and sh*Ctgf* of SM and EM cells (1×10^6) after subcutaneous injection on the back of nude mice ($n = 6$); quantification of tumour volume is shown in the right panel. Ctrl, control (mean ± SEM; $^*p < 0.05$, $^{**}p < 0.005$, $^{***}p < 0.001$). Results are expressed as mean ± SEM and are representative of three independent assays.

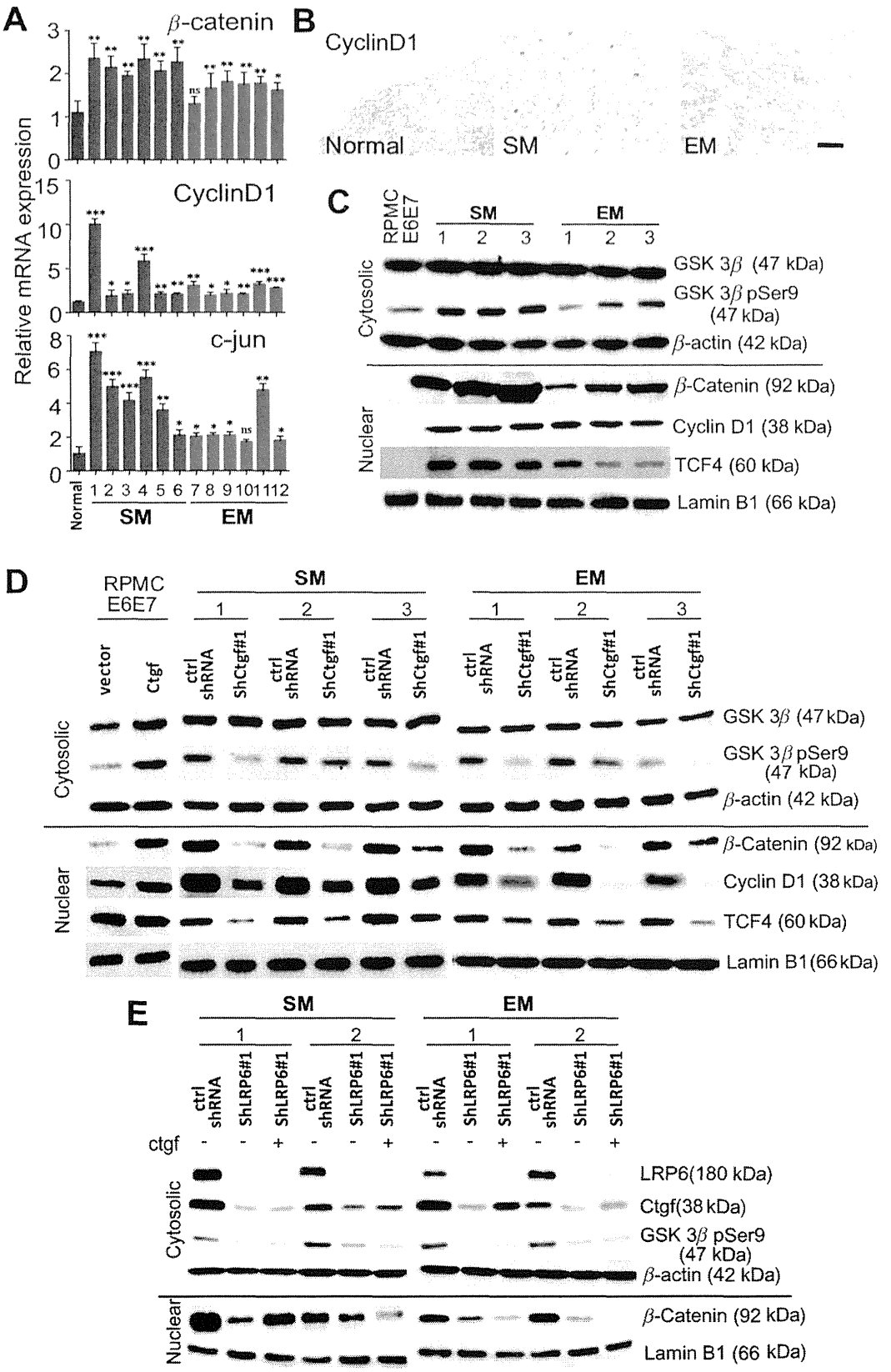

Figure 3. Ctgf stimulates the Wnt-β-catenin-TCF/Lef signalling pathway in rat MM. (A) Quantitative real-time PCR to assess the expression levels of β-*catenin* and its downstream transcription factors *Cyclin D1* and *c-jun*. (B) Immunohistochemical analysis for the evaluation of Cyclin D1; there was higher nuclear immunopositivity in SM than in EM; bar = 50 μm. (C–E) Western blot analysis using cytosolic and nuclear extracts of MM cell lines; Wnt-β-catenin-TCF-Lef signalling regulatory proteins [total GSK3β, phospho(p-Ser9)-GSK3β, nuclear β-catenin, Cyclin D1 and TCF4] were active in both SM and EM (C). This signalling pathway was activated by over-expressing *Ctgf* in non-tumourous cells (RPMCE6E7) and was blocked after knock-down of *Ctgf* in MM cells (D). Furthermore, this signalling pathway was blocked after knock-down of LRP6 in MM cells and did not revive by the addition of recombinant Ctgf (E; 0.5 nM). Results are expressed as mean ± SEM and are representative of three independent assays.

(Invitrogen) and a Real-time PCR System 7300 (Applied Biosystems/Life Technologies) were used with the specific primer pairs (see supplementary material, Table S1). The β-*actin* level was used to normalize the mRNA levels of all genes examined. Each target gene was assayed in triplicate.

Antibodies

All the antibodies used in this study are described in Table S2 (see supplementary material).

Western blot analysis

Protein lysates were prepared by homogenizing the tissue samples in RIPA lysis buffer containing 0.2 mM sodium orthovanadate (Na_3VO_4), 50 mM sodium fluoride (NaF), 1 mM dithiothreitol and 5.7 mg/ml aprotinin. Western blotting was performed as described previously [18,19]. Other methods, including mesothelial cell collection, cell culture, transfection/transduction, RNA interference, colony formation, xenografting and serum determination are described in Supplementary materials and methods (see supplementary material).

Results

Ctgf is over-expressed in asbestos-induced MM, especially in SM

MM has two major histological subtypes, SM and EM, which are reproduced in rats [13,15]. SM consists of elongated spindle cells with a fibroblast-like appearance, whereas EM tumour cells show the characteristics of epithelial cells, with a polarized cuboidal shape and mutual cohesiveness (Figure 1A). To identify genes potentially accounting for the differential prognosis between these two subtypes, we compared the microarray transcriptome profiles of rat asbestos-induced MM (GEO Accession No. GSE48298). *Ctgf* ranked as the top gene with differential expression between SM and EM (Figure 1B; see also supplementary material, Tables S3 and S4). Pathway analysis placed *Ctgf* in the central position for this difference (see supplementary material, Figure S1). We confirmed the results using immunohistochemistry (Figure 1C), quantitative RT–PCR and western blot analysis (Figure 1D). In addition, SM and EM cell lines were established from the ascites of tumour-bearing rats, and their origin was confirmed using three mesothelial markers, podoplanin, calretinin and mesothelin, along with WT1 (see supplementary material, Figure S2). These cell lines showed results consistent with those of corresponding original tumours, with a higher *Ctgf* expression in SM cell lines (Figure 1E). *Ctgf* was over-expressed not only in SM but also in EM, when compared with normal mesothelial cells recovered from the surface of visceral organs or an immortalized rat peritoneal mesothelial cell line (RPMC), suggesting its general potential role in MM.

Ctgf is essential for maintaining the malignant phenotypes of MM cells

To investigate the potential role of Ctgf in maintaining the malignant phenotypes of MM cells, we knocked down *Ctgf* expression in both SM and EM cell lines, using two different shRNA constructs (Figure 2A). Reduced *Ctgf* expression resulted in the suppression of proliferation in both SM and EM, as assessed by two cell proliferation assays (Figure 2B) with Ki-67 expression (see supplementary material, Figure S3) and dead cell fraction (Figure 2C). Moreover, Ctgf-depleted tumour cells displayed a reduced colony-forming ability (Figure 2D). Ctgf depletion also inhibited SM and EM cell invasion in transwell cell invasion assays (Figure 2E). To confirm our findings, we produced cells stably expressing *Ctgf* by infecting EM cells with the pCMSCVpuro–*Ctgf* retrovirus containing full-length *Ctgf*. An empty retrovirus, pCMSCV, was used as a control (Figure 2A). *Ctgf* transduction induced effects opposite to its knock-down, promoting cell proliferation, colony formation and invasion in EM cells (Figure 2B–E). An *in vivo* tumourigenicity assay with nude mice also supported a role for Ctgf in maintaining the malignant potential of MM cells. When injected subcutaneously into nude mice, SM-sh*Ctgf* and EM-sh*Ctgf* cells both showed reduced tumourigenicity compared to control shRNA-infected cells (Figure 2F).

Ctgf activates the oncogenic Wnt–β-catenin signalling pathway in MM cells

Ctgf binds to receptors known as low-density lipoprotein receptor-related proteins (LRPs) [20,21]. As some LRPs also function as a co-receptor of Wnt ligand, we speculated that *Ctgf* over-expression causes a constitutive activation of the oncogenic Wnt–β-catenin signalling pathway. To test our hypothesis, we first measured the mRNA levels of β-*catenin* (*Ctnnb1*) and two major β-catenin target genes, *c-jun* (*Jun*) and *Cyclin D1* (*Ccnd1*), in SM and EM cells. We found increased β-*catenin*, *Cyclin D1* and *c-jun* transcript levels, especially in SM cells (Figure 3A). Immunohistochemical staining of Cyclin D1 also showed higher expression in SM and EM nuclei compared with normal mesothelial cells (Figure 3B). GSK3β (Gsk3β) is an upstream negative regulator of β-catenin activity. By phosphorylating β-catenin, GSK3β prevents nuclear translocation of β-catenin, thereby inhibiting its transcriptional activity. Phosphorylated GSK3β (p-GSK3β; pSer9) is unable to prevent the nuclear translocation of β-catenin [22,23]. We evaluated the phosphorylation status of GSK3β and found a higher level of p-GSK3β in SM and EM cells, with simultaneously increased nuclear protein levels of β-*catenin* and its target genes *Cyclin D1* and *TCF4* (*Tcf4*) [24] (Figure 3C). To further confirm our findings, we knocked down *Ctgf* expression in three SM and three EM cell lines and studied its effects on β-catenin activation. *Ctgf* knock-down resulted in reduced p-GSK3β, reduced β-catenin nuclear translocation and reduced nuclear protein levels of Cyclin D1 and

TCF4 (Figure 3D). In contrast, RPMC over-expressing *Ctgf* showed an activated β-catenin signalling pathway (Figure 3D). The knock-down of LRP6 caused inactivation of the Wnt–β-catenin signalling pathway and reduced *Ctgf* expression. Additional recombinant Ctgf did not reactivate the Wnt–β-catenin signalling pathway when LRP6 was knocked down, suggesting that LRP6 is a major receptor for Ctgf (Figure 3E; see also supplementary material, Figure S4).

Effects of inhibitors for Ctgf and β-catenin on MM

We used FH535 (*N*-2-methyl-4-nitro)-2,4-dichlorosulphonamide) to inhibit β-catenin–TCF and SA3K (SERPINA3K; serine protease inhibitor) to inhibit Ctgf, and evaluated their effects on the phenotypes of MM cells. Both FH535 and SA3K inhibited the activation of β-catenin signalling in MM cells at the protein level in the nuclear fraction, concomitant with decreased cytoplasmic Ctgf, within 24 h (Figure 4A, C). The addition of SA3K eventually suppressed *Ctgf* transcriptional levels (Figure 4B), suggesting the presence of a Ctgf positive-feedback loop. Both FH535 and SA3K inhibited proliferation and invasion of MM cells (Figure 4D, E).

Ctgf induces epithelial–mesenchymal transition (EMT)-like morphological alterations in MM

SM and EM present the characteristics of mesenchymal and epithelial cells, respectively. When we knocked down *Ctgf* expression in SM cells (SM-sh*Ctgf*), we observed a clear morphological alteration from spindle-shaped fibroblast-like cells to cuboidal epithelial-like cells (Figure 5A, upper panel). To confirm our observation, we then retrovirally transduced *Ctgf* into EM cells with low *Ctgf* expression and found an opposite morphological transition from cuboidal to spindle shape (Figure 5A, lower panel). This effect closely resembles the process of EMT, which promotes tumour cell migration, invasion and metastasis [25]. We then investigated the expression level of several EMT markers (*E-cadherin*, *Vimentin*, *Snail*, *Slug*, *Twist1*, *Zeb1* and *Zeb2*) following *Ctgf* transduction or knock-down. E-cadherin (Cdh1) is a marker for epithelial cells, whereas Vimentin (Vim) is a marker for mesenchymal cells. Snail (Sni1), Slug (Sni2), Twist1, Zeb1, and Zeb2 are transcription factors that are known to promote EMT. We found that *Ctgf* knock-down resulted in reduced transcript expression levels of *Vimentin*, *Snail*, *Slug*, *Twist1*, *Zeb1* and *Zeb2* but an increased *E-cadherin* expression. In contrast, *Ctgf* transduction suppressed the *E-cadherin* level but increased those of *Vimentin*, *Snail*, *Slug* and *Twist1* (Figure 5B, C; see also supplementary material, Figure S5). Corresponding changes in E-cadherin, Vimentin, Snail, Slug and Twist1 were also observed at the protein level, as well as in either *Ctgf* knock-down or *Ctgf*-transduced cells (Figure 5D). This EMT-like process was inhibited by the addition of a Ctgf inhibitor (SA3K), as assessed by changes in those EMT markers. The addition of recombinant Ctgf to EM- and SM-sh*Ctgf* cells, in contrast, re-induced *Vimentin*, *Snail*, *Slug* and *Twist 1* expression, which was suppressed with *Ctgf* shRNA (Figure 5D). We showed that activation of the β-catenin signalling pathway is Ctgf-dependent in MM cells (Figure 3). We hypothesized that β-catenin activation might be related to the ability of Ctgf to induce an EMT-like process. We therefore treated two SM and two EM cell lines with a β-catenin inhibitor (FH535). Inhibition of β-catenin activity resulted in a reduction of Vimentin, Snail and Slug levels, especially in SM cells, indicating the involvement of the β-catenin signalling pathway in the Ctgf-induced morphological transition of MM cells (Figure 5E).

Ctgf is autocrine and self-regulatory through a positive feedback loop via the β-catenin signalling pathway

TGF-β signalling was recently reported to activate *Ctgf* transcription in MM cells [26]. We examined the phosphorylated level of Smad2, an important downstream effector of TGF-β signalling, which is activated upon phosphorylation in SM and EM cells. Consistent with previous results [26], TGF-β signalling was activated in MM cells, as evidenced by increased p-Smad2 levels. However, there was no significant difference in the p-Smad2 level between SM and EM cells (see supplementary material, Figure S6A). When we treated RPMC-E6E7 cells with exogenous recombinant Ctgf, there was an increase in the Ctgf protein level in the cellular lysate, with subsequent alterations in the downstream genes (Figure 5D). We here hypothesized that Ctgf is able to regulate its own expression, possibly through the β-catenin signalling pathway, as the *Ctgf* promoter contains a binding site for TCF, the major transcription factor activated by β-catenin. We added β-catenin inhibitor to SM and EM cells and found that the inhibition of β-catenin activity reduced Ctgf protein level in those cells (Figure 4A; see also supplementary material, Figure S6B). In conclusion, these results indicate the presence of a *Ctgf* positive-feedback loop that can be exploited by MM cells to maintain tumour proliferation.

Ctgf is a serum biomarker for the diagnosis of MM

Ctgf is a secretory protein, and both SM and EM tumours produced high levels of Ctgf, with SM tumours producing higher levels (Figure 6A), which were reduced with β-catenin inhibitor (Figure 6B). We then studied whether Ctgf can serve as a serum biomarker for the diagnosis of MM. We measured serum Ctgf and mesothelin levels in 33 rats at day 420 after initial asbestos injection (when there was no sign of MM under close observation). Both markers were significantly higher in the rats that developed clinically obvious MM 384 days later (day 804 following the initial asbestos injection) than in the untreated controls (Figure 7A). These future MM rats showed

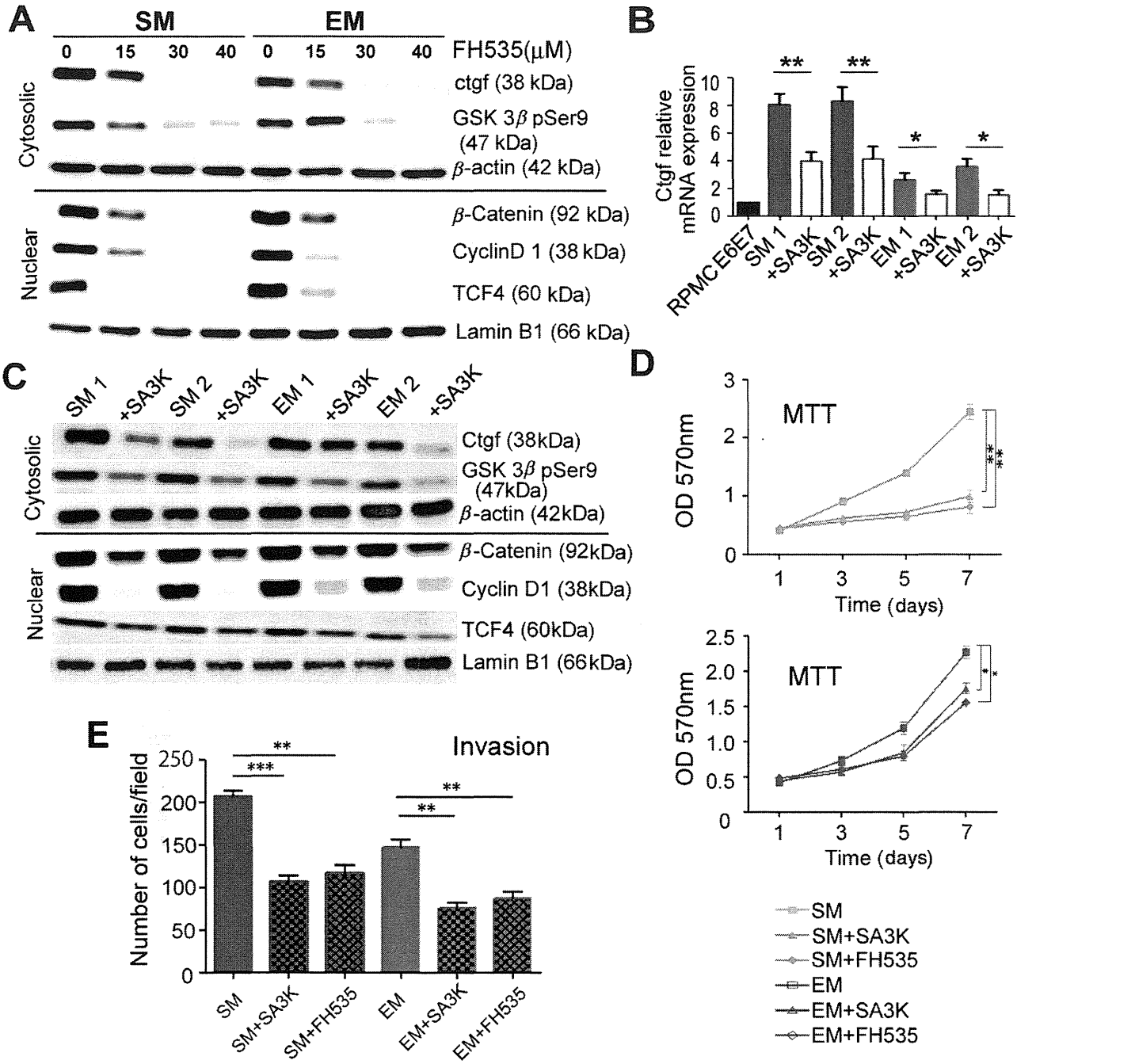

Figure 4. Inhibitors for β-catenin or Ctgf inactivate the Wnt-β-catenin-TCF/Lef signalling pathway. (A, C) Western blot analysis of cytosolic and nuclear fraction from SM and EM cell lines treated for 24 h with 0, 15, 30 or 40 μM β-catenin inhibitor (FH535) (A) or 50 nM Ctgf inhibitor (SA3K) (C). The Wnt-β-catenin-TCF/Lef signalling pathway was inhibited by either β-catenin inhibitor or Ctgf inhibitor. (B) Quantitative real-time PCR analyses showing that the mRNA level of *Ctgf* was reduced 24 h after treatment with Ctgf inhibitor (SA3K; 50 nM). (D) MTT assay for cell viability; cells were subjected to crystal violet staining 1, 3 and 5 days after the addition of SA3K (50 nM) in SM and EM; the experiments were performed in duplicate. (E) Invasion assays to evaluate cell proliferation and invasion after treatment with each inhibitor (mean ± SEM; $^{*}p < 0.05$, $^{**}p < 0.005$, $^{***}p < 0.001$). Results are representative of three independent assays unless stated.

serum Ctgf levels of 37.52 ± 4.83 ng/ml (mean ± SEM, $n = 31$) at 420 days after asbestos injection, whereas control rats showed levels of 2.97 ± 0.56 ng/ml ($n = 7$). Future MM rats showed serum mesothelin levels of 96.06 ± 10.10 ng/ml (mean ± SEM, $n = 31$) at 420 days after asbestos injection, whereas control rats showed levels of 31.53 ± 0.44 ng/ml ($n = 7$). Two rats that were injected with asbestos did not develop MM even at day 812 after the initial injection, which was confirmed by autopsies. These two rats had low levels of Ctgf (2.15 and 2.87 ng/ml) and mesothelin (28.31 and 37.49 ng/ml) at day 420, similar to those in control animals.

In this prospective study, 15 rats that were later identified as having SM via a histological analysis showed significantly higher serum Ctgf levels than those with EM (Figure 7B). These findings were consistent with the fact that SM tumours expressed higher levels of *Ctgf* transcripts. In contrast, serum mesothelin levels were

higher only in rats with future EM tumours and not in those with future SM tumours (Figure 7B). We show in Figure 7C the periods required for these 31 rats in this prospective study from the initial asbestos injection to the days of death/sacrifice due to MM development. The survival of rats was significantly and inversely associated with serum Ctgf levels at day 420 ($r = -0.84$; $p < 0.0001$), which was even more significant when only SM was used for the analyses ($r = -0.89$; $p < 0.0001$). However, serum mesothelin levels were not associated

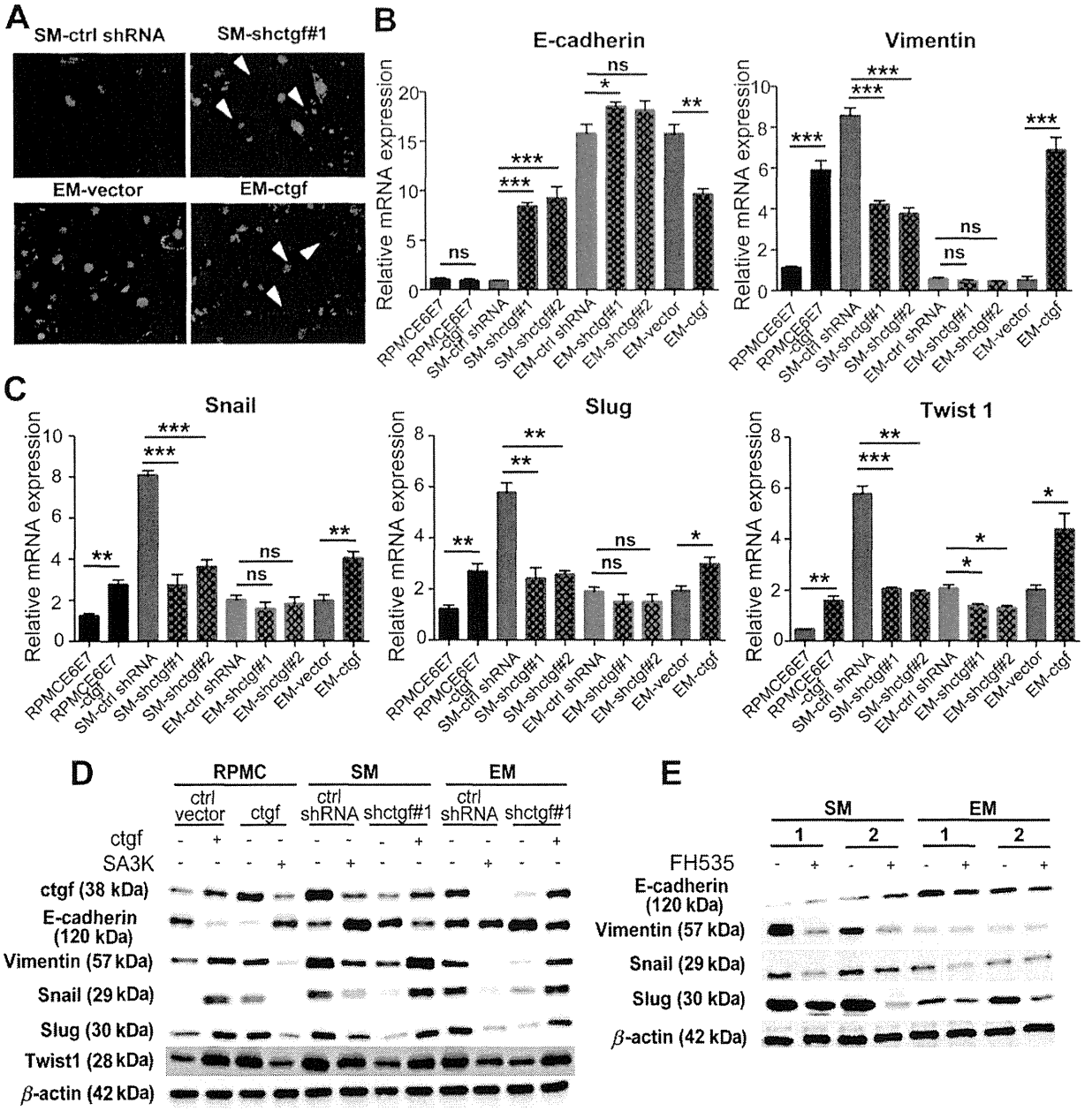

Figure 5. *Ctgf* expression affects MM morphology through its ability to promote an epithelial–mesenchymal transition (EMT)-like process. (A) Actin and DAPI staining of MM cells after transduction; *Ctgf* induces an EMT-like process in *Ctgf*-transduced EM and induces an opposite effect after knock-down of *Ctgf* in SM. (B, C) Quantitative real-time PCR analysis of the mRNA levels of an epithelial cell marker (E-cadherin), a mesenchymal cell marker (*Vimentin*) (B) and the EMT transcription factors *Snail*, *Slug* and *Twist1* (C). The expression of *Vimentin*, *Snail*, *Slug* and *Twist1* was significantly decreased after the knock-down of *Ctgf* and increased after *Ctgf* transduction; E-cadherin showed an opposite effect. (D) Western blot analysis to evaluate the protein levels of Ctgf, EMT markers and EMT transcription factors after various Ctgf manipulations. Ctgf recombinant protein (0.5 nM) or Ctgf inhibitor (SA3K; 50 nM) was added to each cell line; protein was extracted 24 h afterwards, and western blotting was carried out to evaluate the alteration of EMT regulators. The effect of Ctgf inhibitor was indistinguishable from that of *Ctgf* knock-down. Vimentin, Snail, Slug and Twist1 were significantly decreased after the addition of Ctgf inhibitor and increased after the addition of Ctgf recombinant protein; E-cadherin showed an opposite effect. All the results for protein levels were consistent with those of mRNA levels. (E) Effects of β-catenin inhibitor on the EMT-like process. β-Catenin inhibitor (1 μM; FH535) was added to each cell line and protein was extracted 24 h afterwards. Western blot showed that the expression of EMT-associated genes was decreased by β-catenin inhibitor in SM and EM (mean ± SEM; $^{*}p < 0.05$, $^{**}p < 0.005$, $^{***}p < 0.001$; ns, not significant). Results are representative of three independent assays.

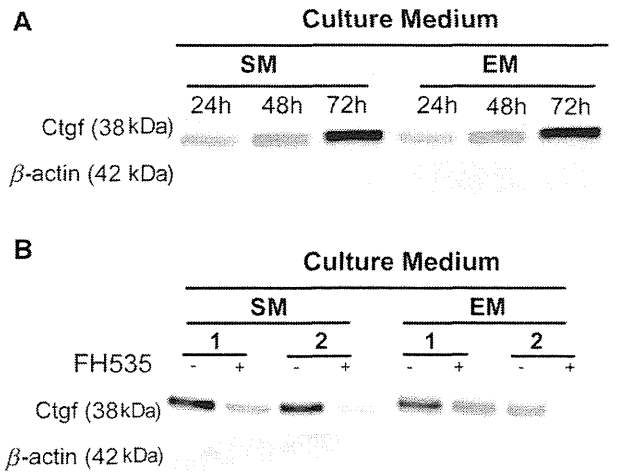

Figure 6. Secretion of Ctgf and its regulation via the β-catenin signalling pathway. (A) Secretion of Ctgf by MM cells into the medium in a time-dependent manner. (B) Effect of β-catenin on the Ctgf secretion of MM cells into the medium. Representative results are shown.

with survival [$r = -0.34$; $p =$ not significant (ns)] either for EM or SM (Figure 7D). The data on each rat are shown in Figure 7E.

Discussion

We identified *Ctgf* as a critical target gene in MM by transcript profiling of two distinct histological subtypes, SM and EM. Ctgf belongs to the CCN family [27]. This family consists of six members, CYR61, CTGF, NOVH, WISP1, WISP2 and WISP3 (CCN1-6, respectively), that all possess an *N*-terminal signal peptide identifying them as secretory proteins and basically four modules in parallel: an insulin-like growth factor-binding domain (module 1); a von Willebrand type C domain (module 2); a thrombospondin-1 domain (module 3); and a C-terminal domain containing a putative cysteine knot (module 4). The current view is that each of the four modules acts both independently and interdependently [20,28]. Modules 3 and 4 of Ctgf bind low-density lipoprotein receptor-related protein (LRP) [29,30] and module 4 also binds heparin [20,31,32]. The biological properties of Ctgf protein involve the stimulation of cellular proliferation, migration, adhesion and extracellular matrix formation and also the regulation of angiogenesis and tumourigenesis [33]. Indeed, an association of CCN proteins with tumour development has been suggested. However, Ctgf has been reported to work as both a tumour promoter and a suppressor, depending on the type of tumour [28,34]. The mechanism of this discrepancy is not well understood at present.

Our present study revealed for the first time that Ctgf promotes the progression of MM through the activation of the downstream Wnt–β-catenin signalling pathway. In addition, activation of the Wnt–β-catenin signalling pathway resulted in a positive-feedback loop through Ctgf secretion and LRP6 stimulation that further increased *Ctgf* expression. Notably, *Ctgf* was up-regulated not only in SM but also in EM when compared with normal mesothelia, suggesting a potentially crucial role for Ctgf in the pathogenesis and malignant phenotype of mesothelioma.

Wnt–β-catenin signalling is a well-known oncogenic signalling pathway, and its activation has been reported in many types of human cancers [23]. Nevertheless, only two studies report the significance of β-catenin in human MM cell lines [35,36], and the association of β-catenin with Ctgf has not been discussed. Because LRP6, a receptor for Ctgf, is also a co-receptor of the Wnt ligand [29], we hypothesized that *Ctgf* over-expression might cause a constitutive activation of the Wnt–β-catenin signalling pathway in MM cells. This hypothesis was supported by the high β-catenin transcriptional activity in SM and EM cells, which was significantly inhibited following *Ctgf* knock-down using shRNA and a specific inhibitor. Moreover, we observed that Ctgf activates β-catenin through the inhibition of GSK3β in MM. GSK3β regulates β-catenin activity via phosphorylation [22]; phosphorylated β-catenin is unable to undergo nuclear translocation and thus is prevented from performing its co-transcriptional activity. Our results here showed that high *Ctgf* expression was associated with a higher level of phosphorylated GSK3β (p-Ser9), which lost its ability to prevent the nuclear translocation of β-catenin. As a result, β-catenin was released to enter the nucleus and activated the transcription of target genes, such as *Ctgf*, *c-jun*, *cyclinD1* and *TCF*, which can promote malignant transformation.

Recently Sekido's group [26] reported findings on the role of Ctgf in MM and how different signalling pathways regulate *Ctgf* expression. They suggested crosstalk between TGF-β and Hippo signalling pathways in the regulation of *Ctgf* expression in MM cells. It is known that the Hippo signalling pathway is frequently inactivated in MM, due to the loss of the tumour suppressor gene *neurofibromatosis 2* (*NF2*) [37]. *NF2* encodes Merlin, which belongs to the ERM protein family. Merlin regulates cell growth through the inhibition of a downstream transcriptional co-activator, Yes-associated protein (YAP). The loss of Merlin function results in YAP activation, which then leads to the enhanced transcription of target genes that promote cell growth and proliferation [38]. The group also observed an activation of the TGF-β signalling pathway in MM, based on an increased level of p-Smad2, an important downstream effector of TGF-β signalling. They then demonstrated that YAP, together with Smad3 and two other molecules (p300 and TEAD), forms a complex that bind to the *Ctgf* promoter region and regulates its expression [26]. Similar to our results, they also found a higher *Ctgf* expression in SM compared with EM. However, they did not observe a significant difference in the activation level of TGF-β signalling between SM and EM, suggesting the presence of an additional activated pathway in the regulation of *Ctgf* expression.

Our present study corroborated their findings by showing the Wnt–β-catenin signalling pathway as an

additional pathway in the regulation of *Ctgf* expression (Figure 8A). In a study of oesophageal squamous cell carcinoma, the *Ctgf* promoter was reported to contain a binding site for the β-catenin–TCF–LEF transcriptional complex [39]. Consistent with this, we found that β-catenin inhibitor was able to down-regulate the expression level of *Ctgf*. In addition, treatment with exogenous recombinant Ctgf revived increased

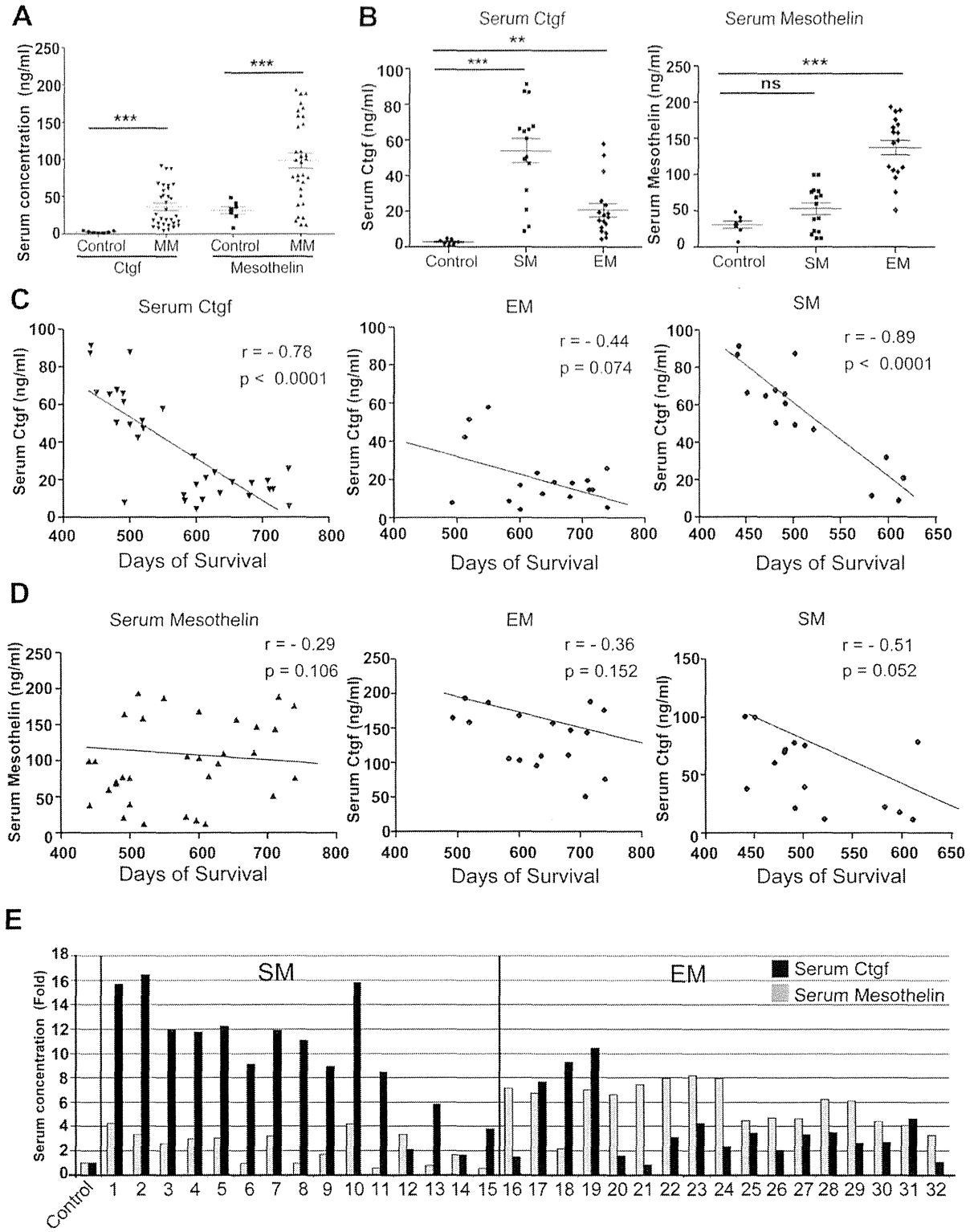

Figure 7. Serum Ctgf level as a biomarker for MM in asbestos-induced rats. (A) Serum levels of Ctgf and mesothelin. (B) Differential serum levels of Ctgf and mesothelin in SM and EM subtypes; see text for details. (C, D) Association of the prognosis of rats with two distinct serum markers in a prospective study. There was a significant proportional correlation between the serum Ctgf and rat survival ($R = -0.78$, $p < 0.001$), but no significant correlation was observed between serum mesothelin and rat survival ($R = -0.29$, p = ns; mean ± SEM; $^{***}p < 0.001$); see text for details. (E) Data of individual rats enrolled in this study.

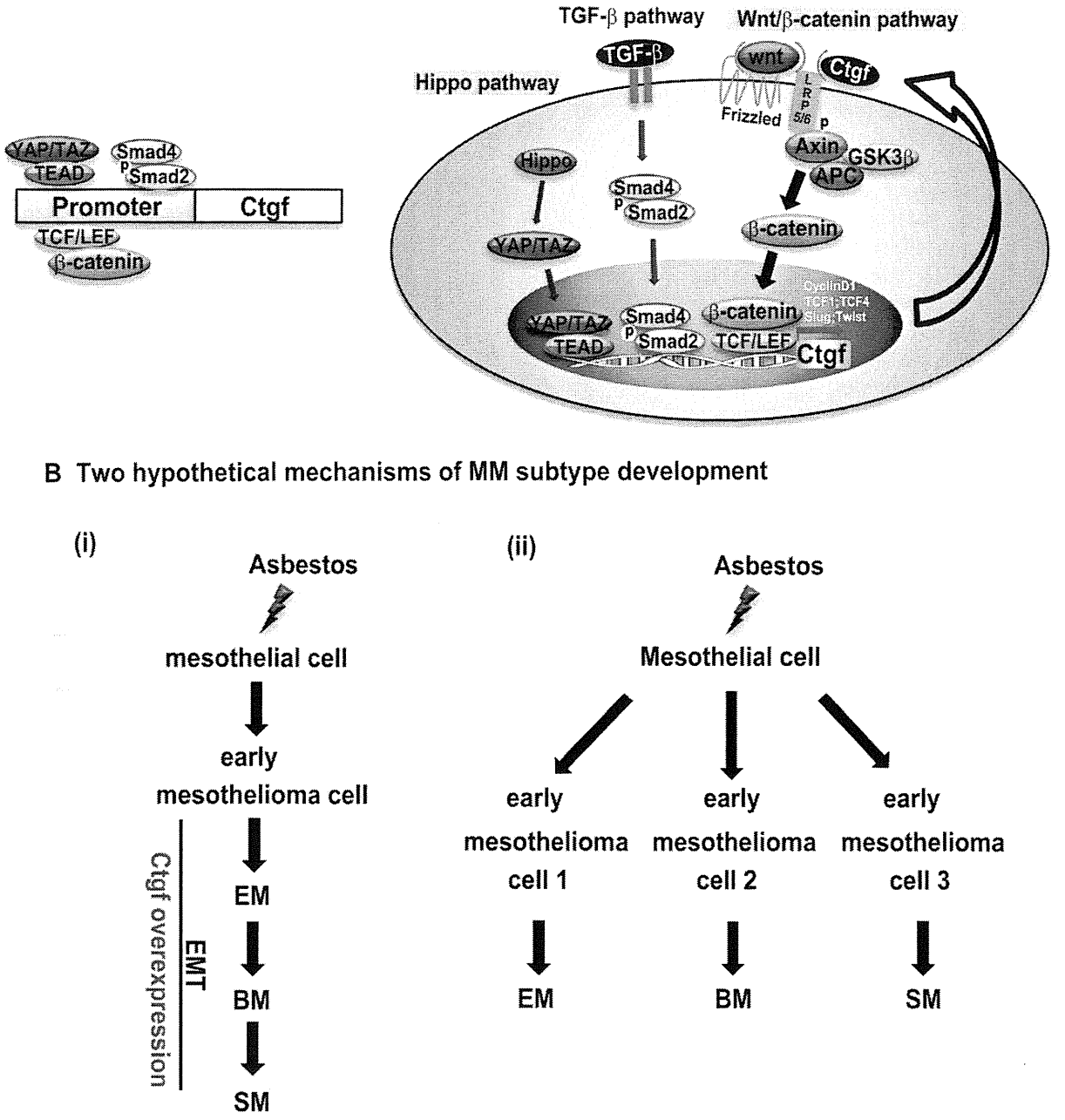

Figure 8. Novel autocrine mechanism between Ctgf and the Wnt–β-catenin–TCF pathway plays a major role not only in EMT in MM but also in the maintenance of malignant potential for all the MMs.

endogenous Ctgf protein levels in MM cells (Figure 5D). Taken together, our data demonstrate the presence of a positive-feedback loop that regulates *Ctgf* expression via the β-catenin signalling pathway in MM cells. Targeting Wnt–β-catenin signalling together with TGF-β and Hippo signalling might be a more effective approach to suppress the oncogenic effects by *Ctgf* in MM cells.

Another interesting finding is that Ctgf can regulate MM cell morphology. EM cells over-expressing *Ctgf* underwent a morphological transition from a cuboidal to a spindle shape, resembling the process of EMT. Here, further study revealed the loss of E-cadherin with an increase in EMT markers, such as *Vimentin*, *Snail*, *Slug* and *Twist 1*. This prompted us to consider the possibility that SM might arise from EM during MM progression through the Ctgf positive-feedback loop (Figure 8B). In fact, a third subtype of MM, BM, exists, which consists of a mixture of both EM and BM subtypes covering more than 10% area. Our results support the hypothesis that BM could represent an intermediate in the transition from EM to SM.

The incubation period for MM after asbestos exposure is 30–40 years, and the number of new patients is still increasing worldwide [4]. Therefore, the identification of serum markers for MM is important. Serum mesothelin, previously referred to as soluble mesothelin-related protein, is currently the most studied and is considered the best available blood protein biomarker of MM [40]. Mesothelin is a differentiation antigen that is normally present on mesothelial cells but is highly expressed in MM (limited to EM) and some other malignancies, including ovarian and pancreatic cancer [40]. In 2003, Robinson *et al* [41] were the first to report serum mesothelin as a biomarker of mesothelioma, using an enzyme-linked immunosorbent assay. This assay later became commercialized as Mesomark (Fujirebio Diagnostics, Malvern, PA, USA) and was approved in 2007 by the US Food and Drug Administration (FDA) to aid in the monitoring of patients with EM and BM. In the present study, serum Ctgf was significantly increased in MM, especially in SM but also in EM, and was remarkably associated with the prognosis of the MM in rats. We propose to use both serum mesothelin and Ctgf as serum biomarkers to further study and better diagnose MM. Studies using human samples are currently in progress in our institute.

In conclusion, our results from preclinical studies provide clear evidence that Ctgf and its associated molecules are crucial in the maintenance of the malignant potential of MM, indicating promising new target molecules, not only for diagnosis but also for novel chemotherapeutic therapies for MM. This may be noteworthy, given a recent report that Ctgf is a therapeutic target in malignant melanoma, another most aggressive tumour in humans [42].

Acknowledgements

We thank members of Toyokuni laboratory for their valuable input and support throughout the study. This work was supported in part by a grant-in-aid for research from the Ministry of Education, Culture, Sports, Science and Technology (MEXT), Japan (Grant Nos 24390094, 221S0001-04 and 24108001) and the National Cancer Centre Research and Development Fund (Grant No. 25-A-5).

Author contributions

LJ and ST conceived and designed the experiments; YY supplied material; LJ, YY, SHC, SA, SU, SW, HN and YO performed the experiments; LJ, SA, TT and ST analysed the data; and LJ and ST wrote the paper.

Abbreviations

BM, biphasic mesothelioma; Ctgf, connective tissue growth factor; EM, epithelioid mesothelioma; EMT, epithelial–mesenchymal transition; LRP, low-density lipoprotein receptor-related protein; MM, malignant mesothelioma; NF2, neurofibromatosis 2; RPMC, rat peritoneal mesothelial cell; SM, sarcomatoid mesothelioma.

References

1. Roggli VL, Oury TD, Sporn TA. *Pathology of Asbestos-associated Diseases*, 2nd edn. Springer: New York, 2004.
2. Huang SX, Jaurand MC, Kamp DW, *et al.* Role of mutagenicity in asbestos fiber-induced carcinogenicity and other diseases. *J Toxicol Environ Health B Crit Rev* 2011; **14:** 179–245.
3. World Health Organization (WHO). Asbestos (chrysotile, amosite, crocidolite, tremolite, actinolite and anthophyllite). In *IARC Monographs on the Evaluation of Carcinogenic Risks to Humans: A Review of Human Carcinogens; Part C: Arsenic, Metals, Fibres and Dusts*. IARC: Lyon, France, 2012; 219–309.
4. Robinson B, Lake R. Advances in malignant mesothelioma. *N Engl J Med* 2005; **353:** 1591–1603.
5. Hodgson JT, McElvenny DM, Darnton AJ, *et al.* The expected burden of mesothelioma mortality in Great Britain from 2002 to 2050. *Br J Cancer* 2005; **92:** 587–593.
6. Delgermaa V, Takahashi K, Park EK, *et al.* Global mesothelioma deaths reported to the World Health Organization between 1994 and 2008. *Bull World Health Org* 2011; **89:** 716–724, 724A–C.
7. van der Bij S, Koffijberg H, Burgers JA, *et al.* Prognosis and prognostic factors of patients with mesothelioma: a population-based study. *Br J Cancer* 2012; **107:** 161–164.
8. Rusch V, Baldini EH, Bueno R, *et al.* The role of surgical cytoreduction in the treatment of malignant pleural mesothelioma: meeting summary of the International Mesothelioma Interest Group Congress, September 11–14, 2012, Boston, MA. *J Thorac Cardiovasc Surg* 2013; **145:** 909–910.
9. Bolukbas S, Manegold C, Eberlein M, *et al.* Survival after trimodality therapy for malignant pleural mesothelioma: radical pleurectomy, chemotherapy with cisplatin/pemetrexed and radiotherapy. *Lung Cancer* 2011; **71:** 75–81.
10. Churg A, Cagle PT, Roggli VL. *Tumors of the Serosal Membranes*. ARP Press: Silver Spring, MD, 2006.
11. Attanoos RL, Dojcinov SD, Webb R, *et al.* Anti-mesothelial markers in sarcomatoid mesothelioma and other spindle cell neoplasms. *Histopathology* 2000; **37:** 224–231.
12. Husain AN, Colby TV, Ordonez NG, *et al.* Guidelines for pathologic diagnosis of malignant mesothelioma: a consensus statement from the International Mesothelioma Interest Group. *Arch Pathol Lab Med* 2009; **133:** 1317–1331.
13. Jiang L, Akatsuka S, Nagai H, *et al.* Iron overload signature in chrysotile-induced malignant mesothelioma. *J Pathol* 2012; **228:** 366–377.
14. Usami N, Fukui T, Kondo M, *et al.* Establishment and characterization of four malignant pleural mesothelioma cell lines from Japanese patients. *Cancer Sci* 2006; **97:** 387–394.
15. Hu Q, Akatsuka S, Yamashita Y, *et al.* Homozygous deletion of *CDKN2A/2B* is a hallmark of iron-induced high-grade rat mesothelioma. *Lab Invest* 2010; **90:** 360–373.
16. Nagai H, Okazaki Y, Chew S, *et al.* Diameter of multi-walled carbon nanotubes is a critical factor in mesothelial injury and subsequent carcinogenesis. *Proc Natl Acad Sci USA* 2011; **108:** E1330–1338.
17. Okazaki Y, Nagai H, Chew SH, *et al.* CD146 and insulin-like growth factor 2 mRNA-binding protein 3 predict prognosis of asbestos-induced rat mesothelioma. *Cancer Sci* 2013; **104:** 989–995.
18. Toyokuni S, Kawaguchi W, Akatsuka S, *et al.* Intermittent microwave irradiation facilitates antigen–antibody reaction in western blot analysis. *Pathol Int* 2003; **53:** 259–261.

19. Tanaka T, Akatsuka S, Ozeki M, *et al.* Redox regulation of annexin 2 and its implications for oxidative stess-induced renal carcinogenesis and metastasis. *Oncogene* 2004; **23:** 3980–3989.
20. Arnott JA, Lambi AG, Mundy C, *et al.* The role of connective tissue growth factor (CTGF/CCN2) in skeletogenesis. *Crit Rev Eukaryot Gene Expr* 2011; **21:** 43–69.
21. Zhou T, Zhou KK, Lee K, *et al.* The role of lipid peroxidation products and oxidative stress in activation of the canonical wingless-type MMTV integration site (WNT) pathway in a rat model of diabetic retinopathy. *Diabetologia* 2011; **54:** 459–468.
22. Dajani R, Fraser E, Roe SM, *et al.* Structural basis for recruitment of glycogen synthase kinase 3β to the axin–APC scaffold complex. *EMBO J* 2003; **22:** 494–501.
23. Clevers H. Wnt/β-catenin signaling in development and disease. *Cell* 2006; **127:** 469–480.
24. Ishitani T, Ninomiya-Tsuji J, Nagai S, *et al.* The TAK1–NLK–MAPK-related pathway antagonizes signalling between β-catenin and transcription factor TCF. *Nature* 1999; **399:** 798–802.
25. Thiery JP. Epithelial–mesenchymal transitions in tumour progression. *Nat Rev Cancer* 2002; **2:** 442–454.
26. Fujii M, Toyoda T, Nakanishi H, *et al.* TGF-β synergizes with defects in the Hippo pathway to stimulate human malignant mesothelioma growth. *J Exp Med* 2012; **209:** 479–494.
27. Perbal B. CCN proteins: a centralized communication network. *J Cell Commun Signal* 2013; **7:** 169–177.
28. Perbal B. CCN proteins: multifunctional signalling regulators. *Lancet* 2004; **363:** 62–64.
29. Mercurio S, Latinkic B, Itasaki N, *et al.* Connective-tissue growth factor modulates WNT signalling and interacts with the WNT receptor complex. *Development* 2004; **131:** 2137–2147.
30. Ren S, Johnson BG, Kida Y, *et al.* LRP-6 is a coreceptor for multiple fibrogenic signaling pathways in pericytes and myofibroblasts that are inhibited by DKK-1. *Proc Natl Acad Sci USA* 2013; **110:** 1440–1445.
31. Gao R, Brigstock DR. Low density lipoprotein receptor-related protein (LRP) is a heparin-dependent adhesion receptor for connective tissue growth factor (CTGF) in rat activated hepatic stellate cells. *Hepatol Res* 2003; **27:** 214–220.
32. Ball DK, Rachfal AW, Kemper SA, *et al.* The heparin-binding 10 kDa fragment of connective tissue growth factor (CTGF) containing module 4 alone stimulates cell adhesion. *J Endocrinol* 2003; **176:** R1–7.
33. Lau LF, Lam SC. The CCN family of angiogenic regulators: the integrin connection. *Exp Cell Res* 1999; **248:** 44–57.
34. Jacobson A, Cunningham JL. Connective tissue growth factor in tumor pathogenesis. *Fibrogen Tissue Repair* 2012; **5**(suppl 1): S8.
35. Uematsu K, Kanazawa S, You L, *et al.* Wnt pathway activation in mesothelioma: evidence of Dishevelled overexpression and transcriptional activity of β-catenin. *Cancer Res* 2003; **63:** 4547–4551.
36. You L, He B, Uematsu K, *et al.* Inhibition of Wnt-1 signaling induces apoptosis in β-catenin-deficient mesothelioma cells. *Cancer Res* 2004; **64:** 3474–3478.
37. Harvey KF, Zhang X, Thomas DM. The Hippo pathway and human cancer. *Nat Rev Cancer* 2013; **13:** 246–257.
38. Sekido Y. Inactivation of Merlin in malignant mesothelioma cells and the Hippo signaling cascade dysregulation. *Pathol Int* 2011; **61:** 331–344.
39. Deng YZ, Chen PP, Wang Y, *et al.* Connective tissue growth factor is overexpressed in esophageal squamous cell carcinoma and promotes tumorigenicity through β-catenin–T cell factor–Lef signaling. *J Biol Chem* 2007; **282:** 36571–36581.
40. Hassan R, Ho M. Mesothelin targeted cancer immunotherapy. *Eur J Cancer* 2008; **44:** 46–53.
41. Robinson BW, Musk AW, Lake RA. Malignant mesothelioma. *Lancet* 2005; **366:** 397–408.
42. Finger EC, Cheng CF, Williams TR, *et al.* CTGF is a therapeutic target for metastatic melanoma. *Oncogene* 2014; **33:** 1093–1100.

SUPPLEMENTARY MATERIAL ON THE INTERNET

The following supplementary material may be found in the online version of this article:

Supplementary materials and methods

Figure S1. Ctgf plays a central role with the differential pathway analysis between SM and EM samples induced by asbestos in rats.

Figure S2. Characterization of malignant mesothelioma (MM) cell lines with immunohistochemistry and western blot analysis confirms their mesothelial origin.

Figure S3. Knock-down of *Ctgf* decreased Ki-67 levels in MM cells with western blot analysis.

Figure S4. Knock-down of a putative Ctgf receptor, LRP6, leads to decrease in Ctgf protein level through the GSK3β pathway.

Figure S5. Knock-down of *Ctgf* leads to decrease in *Zeb1/Zeb2* expression, decrease in a mesenchymal marker (vimentin), decrease in other epithelial–mesenchymal transition (EMT) transcription factors (snail, slug and twist1) but increase in an epithelial marker (E-cadherin).

Figure S6. Equivalent activation of TGFβ signalling in SM and EM subtypes, and regulation of Ctgf through β-catenin.

Table S1. Sequence of real-time PCR primers and *Ctgf* shRNA oligonucleotides.

Table S2. List of antibodies used for western blot analysis and immunohistochemistry.

Table S3. Top 10 genes with significant differential expression between SM and EM.

Table S4. Top 20 up- and down-regulated genes in EM and SM.

IJC
International Journal of Cancer

Expression of chromobox homolog 7 (CBX7) is associated with poor prognosis in ovarian clear cell adenocarcinoma *via* TRAIL-induced apoptotic pathway regulation

Kanako Shinjo[1,2], Yoriko Yamashita[1,3], Eiko Yamamoto[2], Shinya Akatsuka[1], Nozomi Uno[1], Akihiro Kamiya[3], Kaoru Niimi[2], Yuka Sakaguchi[2], Tetsuro Nagasaka[4], Takashi Takahashi[5], Kiyosumi Shibata[2], Hiroaki Kajiyama[2], Fumitaka Kikkawa[2] and Shinya Toyokuni[1]

[1] Department of Pathology and Biological Responses, Nagoya University Graduate School of Medicine, Showa-ku, Nagoya, Japan
[2] Department of Obstetrics and Gynecology, Nagoya University Graduate School of Medicine, Showa-ku, Nagoya, Japan
[3] Department of Experimental Pathology and Tumor Biology, Nagoya City University Graduate School of Medical Sciences, Mizuho-ku, Nagoya, Japan
[4] Department of Pathophysiological Laboratory Sciences, Nagoya University Graduate School of Medicine, Higashi-ku, Nagoya, Japan
[5] Division of Molecular Carcinogenesis, Center for Neurological Diseases and Cancer, Nagoya University Graduate School of Medicine, Showa-ku, Nagoya, Japan

Cancer Cell Biology

Ovarian cancer is the most lethal gynecologic malignancy, and clear cell adenocarcinoma of the ovary (OCCA), in particular, has a relatively poor prognosis among the ovarian cancer subtypes because of its high chemoresistance. Chromobox (CBX) 7 is a polycomb repressive complex 1 component that prolongs the lifespan of normal human cells by downregulating the INK4a/ARF expression which promotes cell-cycle progression. However, recent reports studying the relationship between CBX7 expression and patient survival have differed regarding the tumor cell origins, and the precise role of CBX7 in human carcinomas remains obscure. In this study, we analyzed CBX7 expression by immunohistochemistry in 81 OCCA patients and evaluated its association with their clinical outcomes. Both the overall and progression-free survival rates of the CBX7-positive patients were significantly shorter than those of the CBX7-negative patients ($p < 0.05$). CBX7 knockdown experiments using two OCCA cell lines, TOV21G and KOC-7C, revealed that cell viability was significantly reduced compared to the control cells ($p < 0.001$). Expression microarray analysis revealed that apoptosis-related genes, particularly tumor necrosis factor-related apoptosis-inducing ligand (TRAIL), were significantly upregulated in CBX7 knockdown cells ($p < 0.01$). We further confirmed that CBX7 knockdown resulted in TRAIL-induced apoptosis in the OCCA cells. Thus, in this study, we showed for the first time that CBX7 was associated with a decreased OCCA prognosis. We also successfully demonstrated that the TRAIL pathway is a novel target for CBX7 expression modulation in these cells, and therapeutic agents utilizing the TRAIL pathway may be particularly effective for targeted OCCA therapy.

Ovarian cancer is the most lethal gynecologic malignancy. There is no effective screening method, and most women are diagnosed with advanced-stage disease. In Japan, ovarian clear cell adenocarcinoma (OCCA) accounts for ~25% of all epithelial ovarian cancer (EOC) cases,[1] whereas in North America and Europe, OCCA accounts for only 1–12% of cases.[2] OCCA has been considered to be distinct from high-grade serous adenocarcinoma because of its clinical and biological characteristics. OCCA has been known to be associated with endometriosis,[3,4] and recent studies have suggested that oxidative stress caused by excess iron leads to carcinogenesis in the ovary.[5,6] Advanced stage is associated with poor prognosis in OCCA,[2] and the survival rates in the stages are poorer than those for patients with serous adenocarcinoma,[7] most likely because of OCCA resistance to standard platinum-based chemotherapy.[8] Therefore, it is important to find new therapeutic targets for OCCA.

Chromobox 7 (CBX7) is a member of the polycomb group (PcG) of proteins and is a component of polycomb repressive complex 1 (PRC1). PRC1 can silence the genes that are related to stem cell renewal, differentiation and cancer in conjunction with PRC2.[9] PcG proteins have been reported to be overexpressed and associated with tumorigenesis in a variety of human cancers, mostly by downregulating

Key words: ovarian clear cell adenocarcinoma, chromobox homolog 7 (CBX7), immunohistochemistry, siRNA, expression microarray, TNFSF10 (TRAIL)
Additional Supporting Information may be found in the online version of this article
Grant sponsor: Scientific Research from the Japan Society for the Promotion of Science; **Grant number:** 23590394 (to Y.Y.)
DOI: 10.1002/ijc.28692
History: Received 23 May 2013; Accepted 11 Dec 2013; Online 22 Dec 2013
Correspondence to: Yoriko Yamashita, Department of Experimental Pathology and Tumor Biology, Nagoya City University Graduate School of Medical Sciences, 1 Kawasumi, Mizuho-cho, Mizuho-ku, Nagoya, 467-8601, Japan, Tel.:+81-52-853-8146, Fax: +81-52-842-0817, E-mail: k46581a@nucc.cc.nagoya-u.ac.jp

What's new?

Ovarian cancer is the most lethal gynecologic malignancy, with clear celladenocarcinoma of the ovary (OCCA) having a particularly poor prognosis due to high chemoresistance. Chromobox homolog 7 (CBX7) is a polycomb group transcriptional repressor whose role in human cancer remains controversial. Here, the authors showed for the first time that CBX7 expression is related to worse prognosis in OCCA. Furthermore, knockdown of CBX7 *in vitro* induced apoptosis in OCCA cell lines, possibly via regulation of the TRAIL-pathway. The findings thus indicate CBX7 as a good prognostic marker, andthe TRAIL-pathway as a potential target for OCCA diagnosis and therapy.

the tumor suppressor genes.[10] CBX7 has been reported to extend the cellular life span by directly repressing the INK4a/ARF locus.[11] Additionally, CBX7 is an oncogene in several human tumors, including follicular lymphoma, prostate and gastric cancers.[12–14] In follicular lymphoma, CBX7 also cooperates with MYC to produce highly aggressive B-cell lymphoma and can initiate T-cell lymphomagenesis by repressing the INK4a/ARF locus.[13] Recently, it has been reported that CDKN2B-AS (ANRIL), a long noncoding RNA also encoded in the INK4a/ARF locus, acts together with CBX7 to repress INK4a/ARF locus genes, such as CDKN2A (p16; p16INK4a) and ARF (p14 ARF) in prostate cancer cells.[15] Furthermore, a genome-wide association study comparing Japanese women with endometriosis to healthy controls revealed that a single nucleotide polymorphism that showed the strongest association with endometriosis was located in the intron of the ANRIL gene.[16] As OCCA is known to have strong association with endometriosis,[4–6] we speculated that CBX7 and ANRIL may play some important roles in the OCCA tumorigenesis. However, in clear contrast, the loss of CBX7 expression has been reported in association with poorer prognoses and more aggressive behaviors of pancreatic, colorectal, and lung cancers.[17–19] It has been shown that CBX7 represses CDH1 (E-cadherin) expression and CCNE1 (cyclin E1) expression in pancreatic and lung cancers, respectively.[20,21] Therefore, the role of CBX7 in cancer still remains controversial. In this study, we attempted to clarify the role of CBX7 in ovarian cancer, specifically OCCA.

Material and Methods

Patients and tissue samples

The ethics committee (Internal Review Board) of the Nagoya University Graduate School of Medicine approved the experiments. The human samples were obtained after each patient provided written informed consent. Formalin-fixed, paraffin-embedded tumor samples from 81 primary OCCA were obtained from the patients who underwent surgical treatment at Nagoya University Hospital from 1986 to 2009 and had clinical follow-up information available. Tumor staging was based on the International Federation of Gynecology and Obstetrics (FIGO) classifications, and reviewed by two expert gynecologists (H.K. and F.K.) for this study. All patients were primarily treated with optimally debulking surgery by skilled surgeons in gynecologic oncology. Thereafter, 75 (93%) of the 81 patients received adjuvant chemotherapy. Beginning in 1997, most of the patients received platinum- and taxane-based agents or CPT-11 chemotherapy. Before 1997, various cisplatin-based chemotherapies were administered. The following chemotherapy regimens were followed: 7% cyclophosphamide 500 mg/m^2, adriamycin 50 mg/m^2, and cisplatin 50 mg/m^2 (CAP), 8% cisplatin and carboplatin (PP), 5% cisplatin, vinblastine, and bleomycin (PVB), 62% paclitaxel 175 mg/m^2, carboplatin AUC5 (TC), 3% docetaxel 70 mg/m^2, carboplatin AUC5 (DC), 4% CPT-11 180 mg/m^2, cisplatin 60 mg/m^2 (CPT-P), 2% other, and 9% unknown. Tumor recurrence or progression was determined by clinical, radiologic, or histologic diagnosis. All histologic diagnoses were specifically reviewed by experts in gynecological pathology (Y.Y. and T.N.) for this study. Endometriosis was defined histologically as the presence of endometrial glands and stromal tissues other than the endometrium or within onethird depth of the uterine myometrium. We also excluded ovarian endometrial cysts lacking epithelium without any atypia for the diagnosis of endometriosis.

Cell culture and cell lines

The human OCCA cell line TOV-21G and a prostate cancer PC3 line were obtained from the American Type Culture Collection (ATCC, Manassas, VA), and the KOC7C line was a generous gift from Dr. Junzo Kigawa (Tottori University, Tottori, Japan). These cells were cultured in an RPMI-1640 medium (Sigma-Aldrich, St Louis, MO) containing 10% fetal bovine serum at 37°C under a 5% CO_2 atmosphere and were tested and authenticated using the short tandem repeat (STR) method.[22] Human OCCA cell lines JHOC-5, 7, 8, 9 were recently (2009-) obtained from Riken BRC (Tsukuba, Japan) and cultured using Dulbecco's Modified Eagle's Medium/Nutrient F-12 Ham (DMEM:F12) medium (Sigma-Aldrich) with similar conditions. Human endometrial epithelial cells were obtained from normal endometrium of a patient undergoing hysterectomy, and after collagenase treatment, cells were cultured using DMEM:F12 and then infected first with a lentivirus encoding HPV16 E6 and E7 followed by a retrovirus encoding human telomerase similar to previous studies.[23,24] Establishment procedure for the cells (hEEC-N1) was done with written permission, and established cells were confirmed as endometrial epithelial origin by immunohistochemical

analyses for detection of both keratin and vimentin using similar methods as a previous study.[23]

Immunohistochemistry and RNA fluorescence *in situ* hybridization (RNA-FISH)

For immunohistochemistry (IHC), we used anti-CBX7 (ab21873, Abcam, Cambridge, MA) as the primary antibody. DNA probes for RNA-FISH were prepared by PCR amplifying cDNA templates to obtain ~500 bp sized-PCR products using primers 5′-GAATTTGGGAATGAGGAGCA-3′ and 5′-AAGCTGCAAAGGCCTCAATA-3′ for ANRIL and 5′-TCAG AAGGATTCCTATGTGG-3′ and 5′-TCTCCTTAATGTCAC GCACG-3′ for human β-actin, and then labeled with SpectrumOrange using Vysis Nick Translation Kit (Abbott, Abbott Park, IL). For fluorescence IHC and RNA fluorescence *in situ* hybridization (RNA-FISH), cells were grown on a chamber slide, and fixed with 4% paraformaldehyde. For RNA-FISH, after permeabilization using cytoskeletal buffer, slides were hybridized with the labeled probes. For fluorescence IHC, cells were visualized with Alexa Fluor labeled secondary antibody (Life Technologies, Carlsbad, CA). Finally, cells were counterstained with DAPI and then visualized with a fluorescence microscope.

For formalin-fixed, paraffin-embedded ovarian tumor sections, we used polymer-based methods with the EnVision System (DAKO, Glostrup, Denmark). CBX7 staining was interpreted by three independent pathologists (Y.Y., T.N., and S.T.) blinded to clinical data. Because interobserver variability was rather large in samples with 10–50% nuclear staining, we defined the samples that contained nuclear staining >10% of cancer cells as positive, and the others negative.

Small interference RNA (siRNA) transfection

To knockdown CBX7, we used two individual siRNAs: One was an endoribonuclease-prepared siRNA (esiRNA) against CBX7 (EHU035461, Sigma-Aldrich), and the other was designed using the sense sequence 5′-GCATTTGCCCATC TGCCTT-3′; we named these siRNAs siCBX7-1 and siCBX7-2, respectively. We used MISSION siRNA Universal Negative Control (SIC-001, Sigma-Aldrich) as the negative control. KOC7C and TOV21G were transfected with the siRNAs using the Lipofectamine RNAiMAX reagent (Invitrogen, Carlsbad, CA) at a final concentration of 10 nM, according to the manufacturer's instructions. Analyses were performed 48 hr after transfection.

Quantitative reverse transcriptase-PCR

Total RNA was extracted from the cell lines using the RNeasy Plus Mini Kit (QIAGEN, Hilden, Germany) according to the manufacturer's instructions. Then, cDNA was synthesized from 500 ng total RNA using the Superscript III First-Strand Synthesis System for RT-PCR (Life Technologies), and quantitative PCR was performed as previously described.[25] The sequences of primers were as follows: CBX7, forward 5′-GGATGGCCCCCAAAGTACAG-3′ and reverse 5′-TATACCCCGATGCTCGGTCTC-3′; ANRIL, forward 5′-CAACATCCACCACTGGATCTTAACA-3′ and reverse 5′-AG CTTCGTATCCCCAATGAGATACA-3′; CDKN2A, forward 5′-CATAGATGCCGCGGAAGGT-3′ and reverse 5′-CCCGA GGTTTCTCAGAGCCT-3′; TNFSF10A, forward 5′-C CTCA GAGAGTAGCAGCTCACA-3′ and reverse 5′-GCCCA GAG CCTTTTCATTC-3′; for β-actin, forward 5′-CGGGAC CT GACTGACTA-3′ and reverse 5′-GAAGGAAGGCTGGA AG AGT-3′; and TNFSF10, forward 5′-CCTCAGAGAGTAG CA GCTCACA-3′ and reverse 5′-GCCCAGAGCCTTTTCAT TC-3′. The data from the PCR reaction were normalized against the β-actin expression using the comparative Ct method. The transcripts were quantified in duplicates.

Western blot analysis

Whole-cell or tissue lysates were prepared similarly as previously described[26] from cell lines and primary tumor tissues from four OCCA patients. Twenty-microgram proteins were separated using sodium dodecyl sulfate polyacrylamide gel electrophoresis and blotted on Immobilon P filters (Millipore, Billerica, MA). The following antibodies were used: anti-Cbx7 (1:1,000) (ab21873, Abcam), anti-β-actin (1:2,000) (A5316, Sigma-Aldrich) and anti-PARP (1:1,000) (#9542, Cell Signaling Technology, Beverly, MA). ImmunoStar LD (Wako, Osaka, Japan) was used for chemiluminescence detection.

Cell viability assay

A total of 4,000 cells were transfected with siRNAs in 96-well plates and incubated under 5% CO_2 at 37°C. After 24, 48, 72, and 96 hr, cell viability was assayed by MTS [3-(4,5-dimethylthiazol-2-yl)-5-(3-carboxymethoxyphenyl)-2-(4-sulfophenyl)-2H-tetrazolium] assay using the CellTiter 96 Aqueous One Solution Cell Proliferation Assay kit (Promega, Madison, WI), according to the manufacturer's instructions.

Migration and invasion assay

The assays were performed using 6.5 mm Transwell plates with 8.0 μm pore polycarbonate membrane inserts (Corning Coaster, Rochester, NY). For the invasion assay, the upper surfaces of the filters were coated with 50 μl of matrigel (Becton and Dickenson, Franklin Lakes, NJ). Next, 1×10^5 cells were seeded in the upper chamber in the culture medium without FBS, and the lower chamber contained 10% FBS. The cells were incubated for 24 hr at 37°C in 5% CO_2. After removing the noninvaded or nonmigrated cells, the remaining cells were stained with Giemsa.

Cell cycle analysis

A total of 5×10^5 cells were washed with PBS, fixed with 70% ethanol at −20°C for at least 30 min, washed again with PBS, and incubated with 0.1 mg/ml RNase A solution (QIAGEN) at 37°C for 20 min. The cells were centrifuged, washed again with PBS, and then incubated with 50 μg/ml of propidium iodide (Sigma-Aldrich) on ice for 20 min. The cell cycle profiles were determined using a FACS Calibur

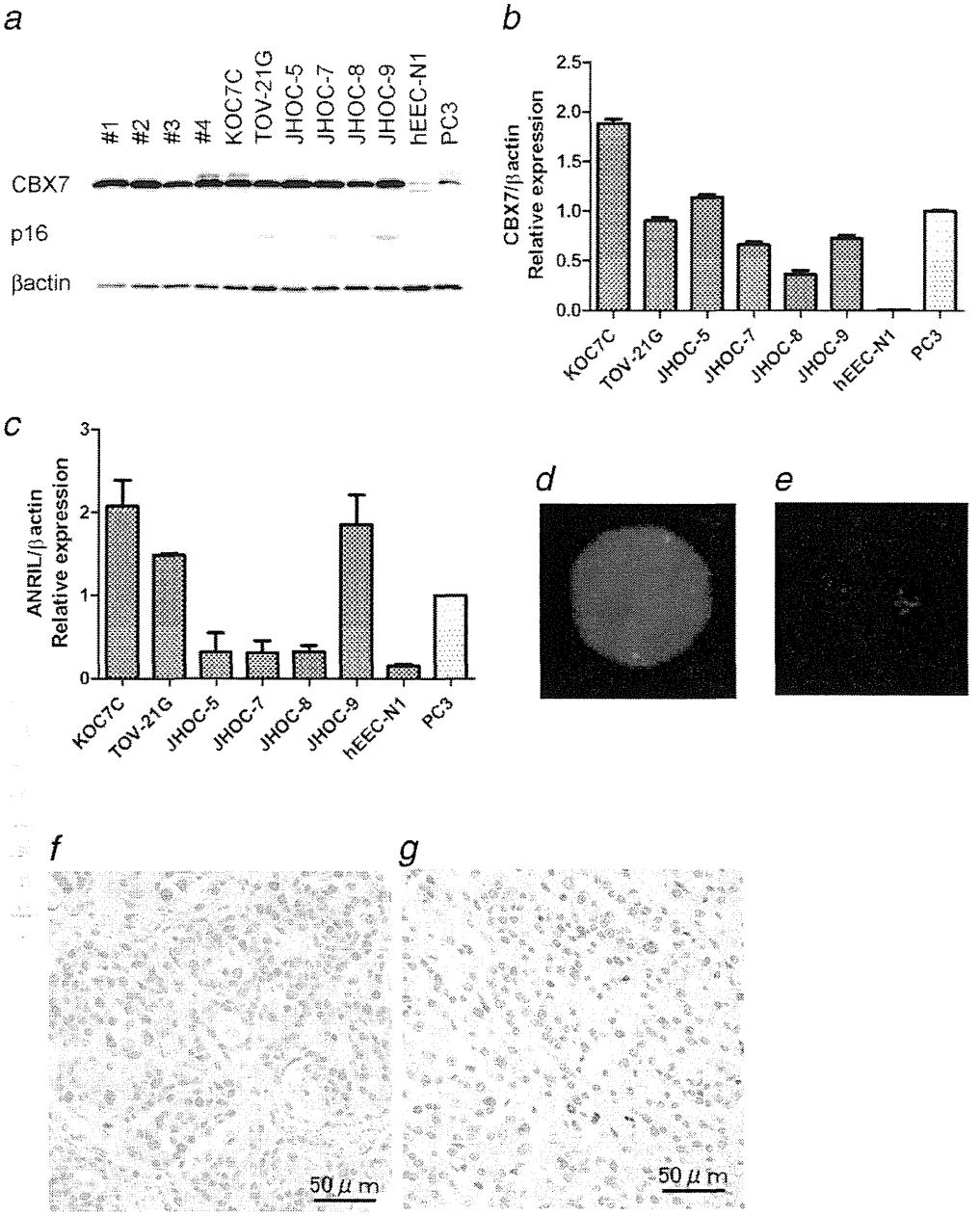

Figure 1. Expression of CBX7 and ANRIL in ovarian clear cell adenocarcinoma (OCCA). (*a–c*) Immunoblotting of four OCCA primary tissue samples (#1,2,3), six OCCA cell lines (KOC-7C, TOV-21G, JHOC-5, -7, -8, -9), a human endometrial epithelial cell line (hEEC-N1) and a positive control prostate cancer cell line, PC3, for detecting CBX7, CDKN2A (p16), and β-actin (*a*). Real-time quantitative reverse transcription PCR analysis using the cells to detect CBX7 (*b*) and ANRIL (*c*). (*d,e*) RNA fluorescence *in situ* hybridization detecting ANRIL (*d*) and fluorescence IHC detecting CBX7 (*e*) in TOV21G cells. Orange signals of both ANRIL and CBX7 are observed in the nuclei of the cells. (*f,g*) Immunohistochemical analysis for CBX7 protein using formalin-fixed paraffin embedded OCCA samples. Intense nuclear staining of the tumor cells is observed (*f*). Negative CBX7 staining (*g*). [Color figure can be viewed in the online issue, which is available at wileyonlinelibrary.com.]

machine (Becton and Dickenson) and analyzed using ModFit LT (Verity Software, Topsham, ME) and CellQuest software (Becton and Dickenson).

Gene expression array analysis

The SurePrint G3 Human Gene Expression 8x60K Microarray (Agilent Technologies, Santa Clara, CA) was used to analyze changes in the mRNA expression levels of the KOC7C and TOV-21G cells after CBX7 knockdown. The microarray targets 27, 958 Entrez Gene RNAs and 7,419 noncoding RNAs. KOC7C and TOV-21G were transfected by siCBX7-1 or negative control siRNA. After 48-hr incubation, total RNA was isolated using the RNeasy Plus Mini Kit (Qiagen). CBX7 knockdown was confirmed by qPCR. Data